(2)

Drag Reduction by Polymer Additives

MITRE

Drag Reduction by Polymer Additives

P. Diamond
J. Harvey
J. Katz
D. Nelson
P. Steinhardt

October 1992

JSR-89-720

JASON
The MITRE Corporation
7525 Colshire Drive
McLean, Virginia 22102-3481
(703) 883-6997

REPORT DOCUMENTATION PAGE

Form Approved
OMB No. 0704-0188

1. AGENCY USE ONLY (Leave blank)	2. REPORT DATE	3. REPORT TYPE AND DATES COVERED
	October 28, 1992	

4. TITLE AND SUBTITLE

Drag Reduction By Polymer Additives

5. FUNDING NUMBERS

PR - 8503A

6. AUTHOR(S)

P. Diamond, J. Harvey, J. Katz, D. Nelson, P. Steinhardt

7. PERFORMING ORGANIZATION NAME(S) AND ADDRESS(ES)

The MITRE Corporation
JASON Program Office A10
7525 Colshire Drive
McLean, VA 22102

8. PERFORMING ORGANIZATION REPORT NUMBER

JSR-89-720

9. SPONSORING/MONITORING AGENCY NAME(S) AND ADDRESS(ES)

Department of Defense
Washington, DC 20301-7100

10. SPONSORING/MONITORING AGENCY REPORT NUMBER

JSR-89-720

11. SUPPLEMENTARY NOTES

12a. DISTRIBUTION/AVAILABILITY STATEMENT

Open for public release; distribution unlimited

12b. DISTRIBUTION CODE

13. ABSTRACT (Maximum 200 words)

The 1989 JASON Summer Study on Drag Reduction focused on the physics which underlies methods utilizing polymer studies. The study included a review of drag reduction phenomenology, the development of continuum models of the dynamics of dilute polymer solutions, the introduction of a simple theory of poly-hydrodynamic turbulence and a discussion of its implications for grid flows, and consideration of optimizing polymer architecture.

14. SUBJECT TERMS

polymerized membrances, turbulent flow, dumbell model, elastic wave

15. NUMBER OF PAGES

16. PRICE CODE

17. SECURITY CLASSIFICATION OF REPORT	18. SECURITY CLASSIFICATION OF THIS PAGE	19. SECURITY CLASSIFICATION OF ABSTRACT	20. LIMITATION OF ABSTRACT
UNCLASSIFIED	UNCLASSIFIED	UNCLASSIFIED	SAR

Contents

EXECUTIVE SUMMARY

The 1989 JASON Summer Study on Drag Reduction focused on the physics which underlies methods utilizing polymer additives. The study included a review of drag reduction phenomenology, the development of continuum models of the dynamics of dilute polymer solutions, the introduction of a simple theory of polymer-hydrodynamic turbulence and a discussion of its implications for grid flows, and consideration of optimizing polymer architecture.

Current experimental evidence from studies of wall streak spacing and wall stress attenuation suggests that drag reduction occurs by the quenching of small scale, high frequency eddys in a buffer layer adjacent to the viscous sub-layer. Theoretical interpretations purport to explain drag reduction in terms of a buffer layer viscosity enhanced by flow-induced polymer uncoiling(G. Ryskin), or in terms of a truncated viscoelastic cascade (P.G. DeGennes and M. Tabor). The uncoiling model is open to question, because it is based on the application of intuition from static extensional flows to fully developed turbulence. The viscoelastic model is incomplete because it fails to consistently account for the ultimate disposition of turbulent eddy energy.

As a foundation for further theoretical and computational study, a set of macroscopic continuum equations which self-consistently describe the fluid and polymer dynamics have been derived. In their simplest form, appropriate to the linear "dumbell" polymer model, these equations describe the dynamics of the polymer extension field and the fluid velocity field, including back-reaction effects due to the presence of the polymers. The continuum model is quite similar to magnetohydrodynamics, with the polymer extension field analogous to the magnetic field. In addition to dissipation due to viscosity and polymer diffusion, a scale-independent damping term, representing the effects of polymer relaxation modes, appears in the extension field equation. We have found the analogy between polymer-hydrodynamic

turbulence and magnetohydrodynamic turbulence quite useful. The extension field is excited by fluid eddy stretching, until elastic energy approaches fluid kinetic energy. This stretching process is limited by polymer relaxation modes at low frequencies.

When excited, the extensional field inhibits the eddy interaction, resulting in a change of the inertial range spectrum from $k^{-\frac{5}{3}}$ to $k^{-\frac{3}{2}}$. Direct calculations then indicate the decay rate of grid polymer-hydrodynamic turbulence exceeds that of ordinary fluid grid turbulence. This is due (primarily) to dissipation due to polymer relaxation modes. Extrapolation to the case of wall flows suggests a picture of a drag-reduced flow as a Newtonian slug with a visco-elastic buffer layer. Enhanced dissipation is due to polymer relaxation modes.

Consideration was given to optimizing polymer architecture for the purpose of drag reduction. While linear chain polymers best meet the dual criteria of low relaxation frequency and high permeated fluid volume fraction (by weight), branched polymers can better resist degradation by distributing (mid-coil) flow induced stresses.

1 OVERVIEW

Polymer drag reduction was discovered about forty years ago by Toms[1], who observed drag reductions of $30 - 40$ percent upon adding only $10ppm$ by weight of polymer(methylmethacrylate) to turbulent monochlorobeneze flowing down a pipe. Similar drag reductions have been observed in polyisobutylene polymer in benzene and cyclohexane. For many applications, the most important solvent is undoubtedly water, for which polyethylene oxide (PEO) produces very similar effects. Minute concentrations of PEO have been used to increase the capacities of irrigation networks, and municipal sewer systems and to extend the range of fire hoses. The drag reducing effects of these polymers are most pronounced when the polymers are flexible with high molecular weights, corresponding to $N = 10^4$ or $N = 10^5$ individual monomer units. Despite the great technological importance of these materials, there is as yet no fundamental understanding of how this remarkable drag reduction is achieved. In this section we briefly discuss the experiments and some important elementary facts about polymer sizes and relaxation rates. Some novel chemical architectures for polymer additives are discussed. Section 2 is a critique of existing ideas about polymer drag reduction. In Section 3.1 we discuss macroscopic continuum models of dilute solutions of polymers modeled as stretchable dumbells. In Section 3.2, we discuss the dynamics of polymer-hydrodynamic (PHD) turbulence. The continuum model presented in Section 3 can be analyzed using methods familiar from studies of turbulent magneto-hydrodynamics. The analysis suggests interesting and non-trivial modifications of the Kolmogorov turbulence theory. A prediction of the energy dissipation rate for grid PHD turbulence is given, and its implications for pipe flow discussed. Section 4 contains our program recommendations. The basic phenomenology of MHD turbulence is reviewed in the Appendix.

1.1 Phenomenology of Drag Reduction

A typical experimental result[2] is shown in Figure 1-1. For a fluid with density ρ and average velocity $< v >$ flowing down a pipe of diameter D the figure of merit is the mass flux

$$Q = \frac{\pi D^2}{4} \rho < v > \qquad (1-1)$$

obtained for a given pressure head Δp. A dimensionless measure of the ratio of pressure head to mass flux is the "friction factor"

$$f = \frac{D\Delta p}{2\rho < v >^2} \qquad (1-2)$$

which is $f = 16/Re$ for laminar flows with Reynolds number $Re = D < v > /\mu$. Although the addition of small amounts of PEO polymer has no observable effect in the laminar regime, there is a striking change in the drag above the transition to turbulence which occurs for $Re \approx 2500$ obtainable with as little as $5ppm$ (by weight) of additive. The effect increases with increasing polymer concentration.

It is well known that enhanced drag in turbulent, high Reynolds number flows is caused by radial transport of flow momentum by fluid eddys. Standard pipe flows are well described by the Prandtl mixing length theory[4], in which the flow is sub-divided into a viscous sublayer near the wall and an inertial layer extending to the core of the pipe. In the viscous sublayer ($0 < x < \nu/U_*$, where ν is the fluid kinetic viscosity and U_* the friction velocity), the flow profile is linear ($U = U_*^2 x/\nu$) and all eddys fall in the dissipation range. In the inertial layer ($\nu/U_* < x$), the flow profile follows the logarithmic "Law of the Wall" $U = (U_*/\kappa)\ell n x$ (κ is the von Karman constant), with a spectrum of turbulent eddys of size $\nu^{3/4}x^{1/4}/U_*^{3/4} < \ell < x$ to be found at each distance x from the wall. At the onset of polymer drag reduction, an elastic buffer layer adjacent to the viscous sublayer arises. Within the buffer layer, the flow profile steepens relative to the Newtonian logarithmic profile, resulting in the formation of a region of "effective slip" (i.e. reduced momentum transport). It is interesting to note that in the buffer layer, fluctuating

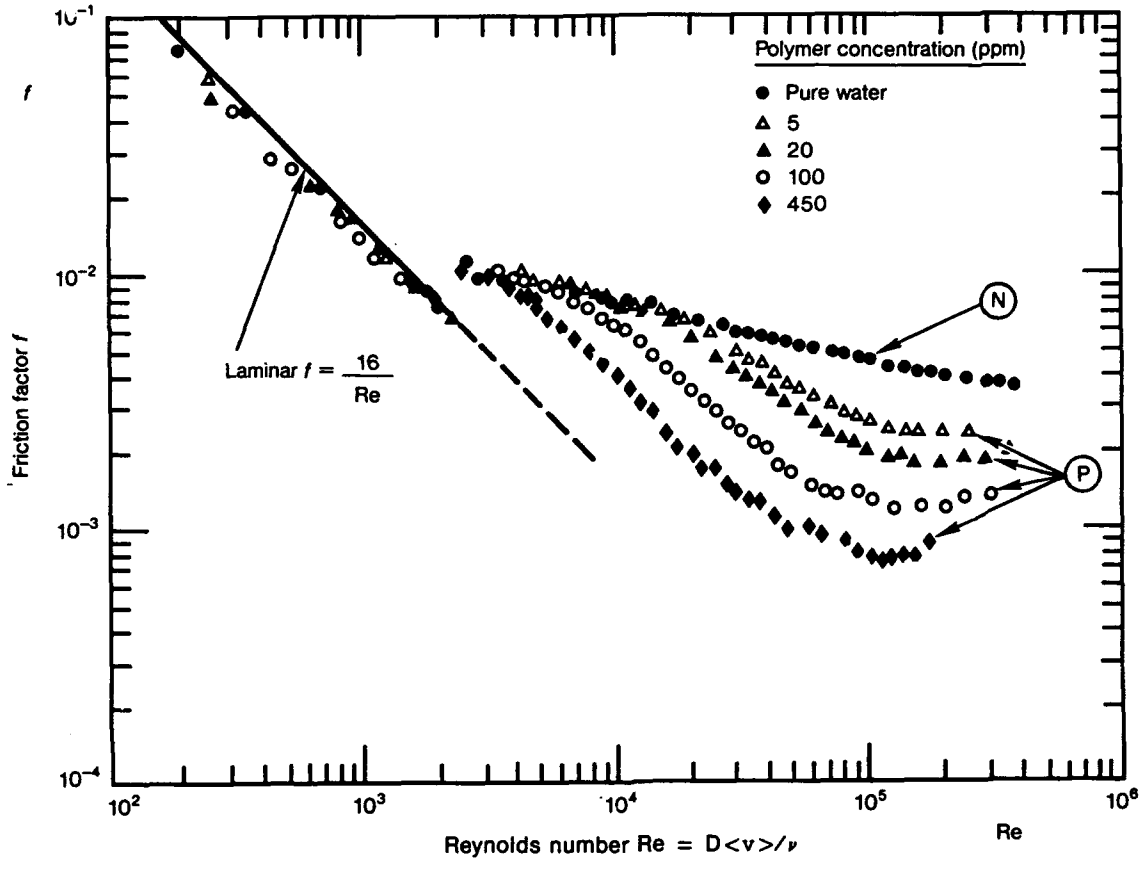

Figure 1-1. Plot of the "friction factor" defined in the text as a function of Reynolds number for turbulent water flowing in a pipe with various concentrations of PEO. Points labelled "N" are with no polymer additives, while points labelled "P" have polymers in varying concentrations; from Ref. [2]

radial velocities are smaller than their Newtonian counterparts, but fluctuating axial velocities actually increase! However, radial and axial velocities tend to decouple in drag reduced flows, so that $< VU >$ decreases and the net turbulent transport of momentum is reduced[3]. Note that the increase in axial fluctuation energy is consistent with the formation of a region of enhanced slip. As drag reduction increases, the buffer layer expands toward the center of the channel while the inertial layer shrinks. It is important to keep in mind that the viscous sublayer remains intact throughout the drag reduction process. Thus, drag reduced flows can be viewed as a Newtonian plug, connected to the viscous sublayer by an elastic buffer layer which supports enhanced slip.

It is worthwhile to comment on the observations pertaining to the onset of drag reduction. Experimental studies indicate that a critical wall shear stress σ_w is required for the onset of drag reduction, and that σ_w is independent of pipe diameter, solvent density, or viscosity. A dependence of σ_w on polymer gyration radius (defined in Section 1.2) R_G of the form $\sigma_w \sim R_G^{-\alpha}$ is observed, with $2 < \alpha < 3$. The gyration radius R_G is virtually always significantly smaller than the dissipation scales of turbulent flows of Reynolds numbers $Re < 10^6$.

There are also experiments[5] which monitor the friction factor as a function of the distance downstream from a point in the center of the pipe where the drag reducing agent is injected. Some drag reduction appears even before significant amounts of additive have had time to diffuse to the wall. One (controversial) interpretation of these experiments is that polymers do not merely lubricate the boundary layer at the wall but also act to modify the approximately homogeneous isotropic turbulence in the center of the pipe. We are unaware of experiments on changes induced by polymers added to grid-generated turbulence, away from walls, which could clarify this point.

1.2 Elementary Facts About Polymers

To get some feeling for the ways in which polymer additives might affect turbulent flow, we need to estimate their characteristic size and time scale[6]. A simple random walk model of a polymer chain with N monomer units, which ignores the interactions between different monomers, predicts a size or "radius of gyration" R_g which grows like $N^{\frac{1}{2}}$,

$$R_g \approx aN^{\frac{1}{2}}, \qquad (1-3)$$

where a is the monomer size. A more accurate formula, which takes into account swelling due to self-avoiding interactions between monomers is,

$$R_g \approx aN^{\frac{3}{5}}. \qquad (1-4)$$

The chemical formula for polyethylene oxide with N monomers is

$$\ldots[-CH_2 - CH_2 - 0-]_N \ldots. \qquad (1-5)$$

Each monomer unit is about $a \approx 5\mathring{A}$. The density of polymeric material with $N = 10^4$ inside a cube with edge R_g centered on this very tenuous object is thus only $4 \times 10^{-4} g/cm^3$!. This remarkably low density of monomer means that no water molecule is ever very far from a flexible polymer chain even at very low concentrations of chains. The volume, for example, enclosed by the radii of gyration of 1.4×10^{14} PEO molecules with $N = 10^4$ added to one cubic centimeter of water (corresponding to a concentration of $100ppm$ by weight) is about 25 percent of the available volume.

Each polymer chain is a delicate little mechanical transponder, with its own set of internal relaxation times, which reacts to the stresses associated with fluid motion. Although the spectrum of relaxation times of a polymer in a solvent is complicated, the *slowest* dynamical mode is associated with distortions of the (approximately spherical) equilibrium polymer shape and is known to be[6]

$$\tau_z \approx \frac{\eta_s R_g^3}{k_B T} \sim N^{1.8} \qquad (1-6)$$

where η_s is the solvent viscosity. The important time scale τ_z is called the "Zimm time" and is of order milliseconds for PEO with $N = 10^4$ monomer units. To within numerical factors, it can be written as[6]

$$\tau_z \approx \gamma/K \qquad (1-7)$$

i.e., as the ratio of the Stokes drag coefficient $\gamma = 6\pi\eta_s R_g$ for a slightly stretched polymer of characteristic size R_g and a Hookean force constant $K = k_B T/R_g^2$. Temperature appears in the effective polymer spring constant because the restoring force for a stretched polymer is entropic in origin, due to the many more configurations available to a polymer in its coiled, as opposed to stretched state.

When polymers interfere with turbulence, it is because they distort in the fluctuating velocity field and eventually react back on the flow. The approximately $1200\mathring{A}$ size of a typical polymer is much smaller than the Kolmogorov inner scale for most turbulent flows. Thus the polymers see an effectively uniform random straining field from all the eddies in the cascade. The Zimm time determines which eddies will have a strong effect on the polymers since they will quickly reassume their equilibrium shape in response to strains induced by an eddy of size l unless the eddy turnover time is shorter than τ_z. The strain rate $\dot{\gamma}(l)$ (i.e., the inverse eddy turnover time) for an eddy of size l within the Kolmogorov theory is well-known to be

$$\dot{\gamma}(l) = \epsilon^{\frac{1}{3}}/l^{\frac{2}{3}}. \qquad (1-8)$$

The only eddies in the turbulent cascade which will be able to distort the polymer shape are those for which[7][8]

$$\dot{\gamma}(l)\tau_z > 1, \qquad (1-9)$$

i.e., those eddies with $l < l^*$, where

$$l^* = (\epsilon\tau_z^3)^{\frac{1}{2}} \sim \epsilon^{\frac{1}{2}} N^{2.7}. \qquad (1-10)$$

It is appropriate to interject here that the observation that a critical wall Reynolds stress must be exceeded for drag reduction to result is closely

related to the time criterion expressed by Equation (1-9). This is easily seen by noting that for wall flows, the maximal eddy shearing rate is $\dot{\gamma} = U_*^2/\nu = U_*/x_\nu$, where $x_\nu = \nu/U_*$ is the width of the viscous sublayer. Thus, drag reduction will occur if $U_*/x_\nu > \tau_z^{-1}$, which is equivalent to $U_*^2 > \nu/\tau_z$. This is equivalent to the condition that

$$\tau_w = \rho U_*^2 > k_B T/R_g^3, \qquad (1-11)$$

which defines a critical wall Reynolds stress varying inversely with R_g^3 and which is independent of solvent density, viscosity and pipe radius.

The length scale l^* is independent of the polymer concentration, and is of order $10^{-2}cm$ for a typical $\epsilon \approx 10^6 cm^2/sec^3$. Possible consequences of the polymer distortions induced by eddies smaller than this scale but larger than the Kolmogorov inner scale l_d will be discussed in Sections 2 and 3. Here, we simply note that strongly stretched polymers will begin to react back on the flow on those scales $l, l_d < l < l^*$, when the restoring forces per unit volume are comparable to the Reynold's stresses in the turbulent fluid[8]. For "ideal" polymers, whose equilibrium size is given by Equation (1-3), the restoring force f for a single polymer is linear in the distorted polymer size Q[6],

$$f = KQ = k_B T Q/R_g^2. \qquad (1-12)$$

Here, K is the Hookean spring constant discussed above, and Q, (see Section 3) can be defined in terms of a hydrodynamic average of a stretching vector describing the distortion of each polymer. Note that the energy associated with this force, $E = \frac{1}{2}KQ^2$, is comparable to the thermal energy $k_B T$ when $Q = R_g$. This result applies only for weak distortions of polymers. The force will be much larger when the polymer is fully extended, i.e., for $Q \sim Na$. When excluded volume interactions are taken into account, there is also an intermediate regime of stretching, $R_g << Q << Na$, for which[6]

$$f \approx k_B T Q^{\frac{3}{2}}/R_g^{\frac{5}{2}}. \qquad (1-13)$$

A complete theory of polymer drag reduction must determine how the non-linear springs embodied in Equation (1-13) alter the flow which stretch them. The construction of such a theory is a formidable challenge; as we shall see in Section 3, the hydrodynamics of turbulent flows in which the polymers behave as linear, Hookean springs is already quite nontrivial.

1.3 Branched Polymers and Polymerized Membranes

The simple ideas sketched above allow us to estimate whether the synthesis of polymers with novel, nonlinear architectures would be useful in turbulent drag reduction. It is possible to synthesize branched polymers, for example, whose connectivity is illustrated in Figure 1-2. There is currently considerable interest in the other novel architecture shown in Figure 1-2, that of polymerized membranes[9]. These flexible "tethered surfaces" assume configurations in a solvent not unlike crumpled pieces of paper.

Upon first consideration, branched polymers and polymerized membranes appear to be disadvantageous compared with linear polymers. The key relation is the scaling of the radius of gyration, R_g, with the number of monomer units, N:

$$R_g \approx a' n^{\nu}; \qquad (1-14)$$

here n is the number of nodes in a branched polymer or tethered surface, and a' is proportional to $m^{3/5}$ where m is the average number of monomers per nodes ($mn \approx N$). The exponent, ν, is approximately, 0.5 for branched polymers[10], and 0.4 for polymerized surfaces[9].

For fixed N, the radius of gyration decreases as the number of nodes increases, which makes the polymer less effective in drag reduction. One wishes to increase the Zimm time as much as possible so as to 'activate' the polymers by eddy-induced stretching at increasingly larger onset scales given by (see Equation (1-10)), $\ell_z \sim \epsilon^{1/2} R_g^{9/2}/(k_B T)^{3/2}$. Yet, the Zimm time is proportional to R_g^3, and hence is shorter (for fixed N) for branched polymers or tethered surfaces compared to linear polymers. Second, one wants to permeate a significant fraction of the fluid with polymer even though they are a negligible component by weight. The relevant figure of merit is the mass density of monomer inside the radius of gyration.

$$\rho \approx \frac{M_0}{N_a}\left(\frac{N}{R_g^3}\right) \sim N^{1-3\nu}, \qquad (1-15)$$

where M_0 is the monomer molecular weight and N_a is Avogadro's number. For a fixed number of monomers, N, the cheapest additives will be those

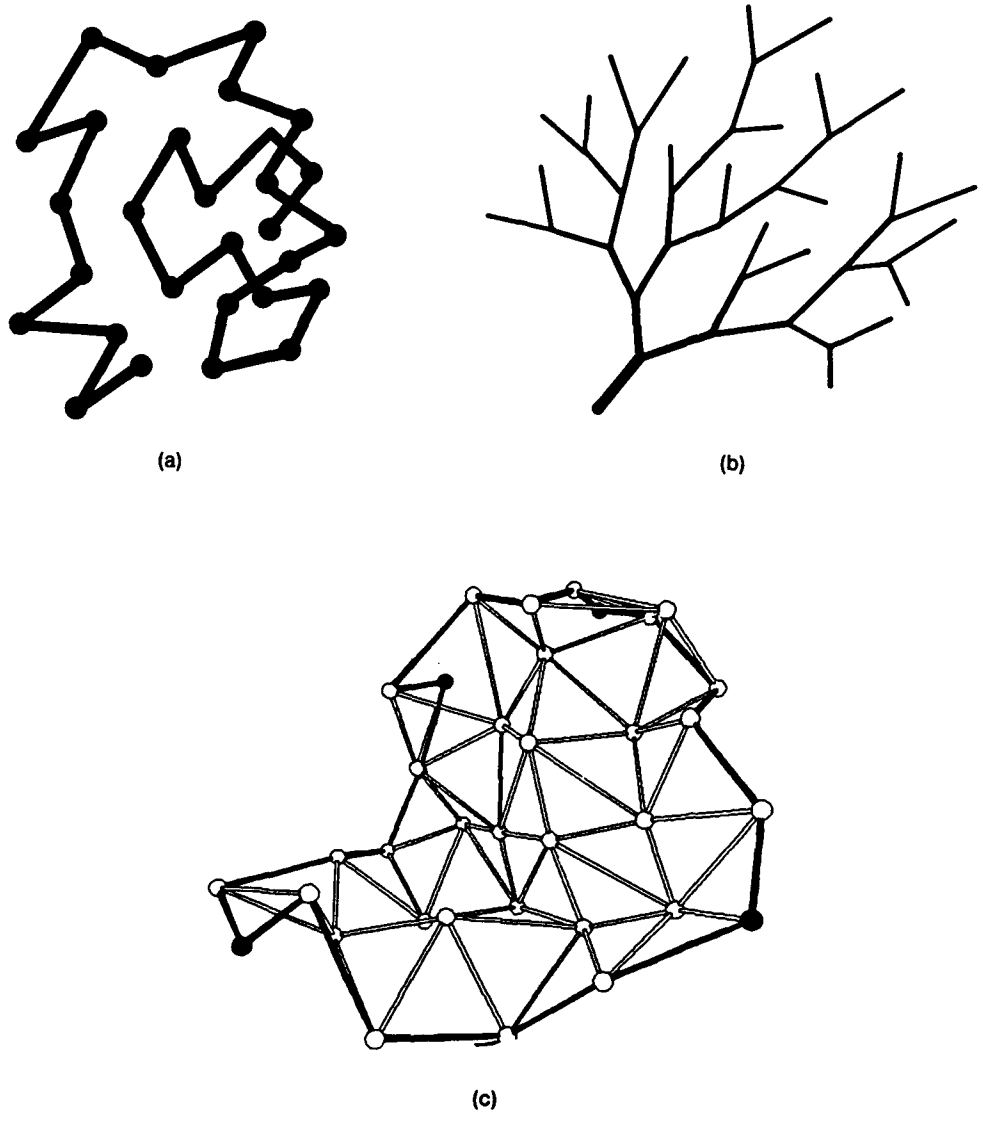

Figure 1-2. Various chemical linkages which could be used for turbulent drag reduction: (a) conventional linear polymer; (b) Branched polymer characterized by a fixed ratio of branch points to monomer units; (c) A polymerized membrane, with the internal connectivity of a flat two dimensional surface. Such surfaces can be made more flexible by connecting the nodes with polymer chains, as in a two dimensional gel.

which produce the most tenuous structures, i.e., those with the lowest value of ρ or the largest ν. Not surprisingly, linear polymers are also most efficient from this point of view.

However, branched polymers or tethered surfaces have the potential advantage that they will be less susceptible to degradation at high Reynolds numbers. When linear polymers are fully stretched in the extensional flow fields, they break (usually near the center) and become less effective in reducing drag. To appreciate this effect, let us model the stretched linear polymer as a set of spheres of radius b connected by springs with spring constant k, as shown in Figure 1-3. We will assume that the polymer is stretched linearly along the x-direction by an extensional flow field, $v_x = \dot{\gamma}x$, as might be created locally by turbulent eddies, and that the flow field is centered on the middle of the polymer. If only the spheres interact hydrodynamically with the flow field, the net force on the n^{th} sphere is

$$F_n = k\delta_{n-1} - k\delta_n - 6\pi\eta b\dot{\gamma}x_n, \qquad (1-16)$$

where $n = 0$ is the center of the polymer, x_n is the position of the n^{th} sphere, $\delta_n \equiv x_{n+1} - x_n - \bar{x}$ is the extension of the n^{th} spring from its equilibrium length $\bar{x}$, and μ is the viscosity of the fluid. In equilibrium, $F = 0$. One immediately observes that $\delta_{n-1} > \delta_n$; in other words, springs closer to the center of the polymer are stretched more. If we take the continuum limit, replacing n by the continuous variable s, Equation (1-16) becomes

$$\frac{d\delta(s)}{ds} = -\alpha x(s), \qquad (1-17)$$

where $\alpha = 6\pi\eta b\dot{\gamma}/k$. Near the center of the spring, $ds \propto dx$, so Equation (1-16) has the solution $\delta \sim (\alpha/2)(L^2 - x^2)$, indicating a parabolic falloff in the tension as one moves away from the center of the polymer. This argument may explain why experiments on polymer degradation at ultrahigh strain rates indicate breaking near the middle of the chain.

The branched polymer illustrated in Figure 1-3 (or a tethered surface) may alleviate the degradation problem. Let us first suppose that the branched polymer is arranged so that the end with fewer branches is furthest away from

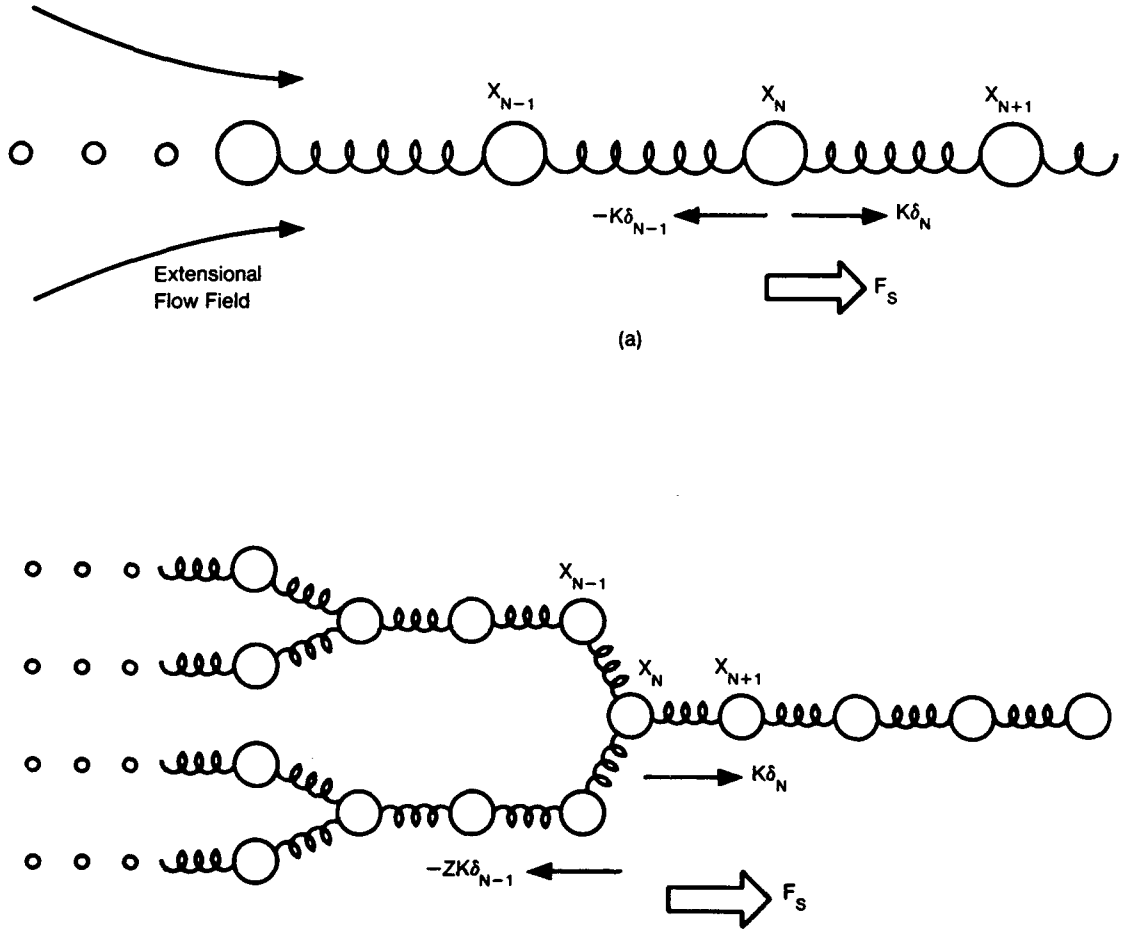

Figure 1-3. Polymer ball-and-spring model in a high Reynolds number extensional flow field, $v = \dot{\gamma}x$. The center of the polymer is at $x = 0$ and all springs are stretched nearby along the x-axis. F_S is the stoker drag on the Nth ball, $F_S = 6\pi\eta b\dot{\gamma}x_N$. [(a) Linear polymer (b) Branch polymer.]

the center of the extensional flow field (see remarks below). The tension increases as one proceeds inwards from the end of the polymer until one reaches a node. At the node, there are two (or more) polymer strands which share the load; that is, the coefficient of the first term in Equation (1-15) is multiplied by two (or more), so now δ_{n-1} may be less than δ_n. Adding more nodes as one proceeds closer to the center of the flow field continues to limit the tension, and, hence, avoids degradation at higher Reynolds numbers. Given that the radius of gyration decreases as the number of nodes increases, one wishes to have the minimum number of nodes necessary to avoid degradation at the design Reynolds number.

In simple models, branched polymers begin from linear chains that grow out from a central core and then bifurcate after some fixed average number of monomer units; the branches then bifurcate after growing and extending a similar number of monomer units, etc. If such a branched polymer were placed in an extensional flow field with the central node in the middle, the effect would be the opposite of that described above. The tension on the monomers in the many distant limbs would be focused on the central node. This may not be a real problem since this would merely cause the original branches to snap from the central node, in which case each fragment would be similar to the cartoon in Figure 1-3. However, it remains unclear whether the fragments will align themselves in the flow field so that the branch that was central originally moves to the farthest part in the flow field.

Polymerized surfaces may be better candidates in that their behavior is more predictable. We might envisage the surface as a square grid of polymer chains meeting at nodes. In an extensional flow field, the grid will deform into an extended, nearly linear configuration with the corners, say, furthest from the center of the extensional flow field. As with the branched polymers, the nodes in the grid can limit the tension on segments near the center of the flow field. The disadvantage of polymerized surfaces compared to branched polymers is that ν is smaller. However, if the grid is rather sparse (few nodes), this may not be so significant.

In conclusion, it appears that the application of polymers with novel

architectures is a possible mechanism for extending polymer drag reduction to flows with very high Reynolds number. The addition of crosslinks helps the ploymers resist degradation, but also means that greater concentrations of polymers are necessary to obtain the same drag reduction.

2 THEORIES OF DRAG REDUCTION

2.1 An Overview of The Problem

Drag reduction by polymers in turbulent flows is an extremely complicated problem. It combines the complexity of turbulent flow (difficult even for a Newtonian fluid) with the problems of polymer physics; their combination changes the character of the turbulence and leads to a yet more complex and difficult problem.

A naive attempt to understand the effects of polymers on drag could go astray in any one of several ways. Dissolved polymers increase the viscosity of polymer solutions, particularly if the polymer molecules are extended; it might therefore be (incorrectly!) inferred that they would increase drag (albeit slightly), just as would an increase in the viscosity of a pure Newtonian solvent, even at high Reynolds numbers. The fact that in turbulent flows the observed effect is in the opposite direction is sufficient to establish the subtlety of the physics involved. So long as the flow remains laminar, the naive drag increase is expected to be correct; however in laminar flow the polymers usually remain coiled so this effect would be very small. It instead might be supposed that polymers could have no effect at all on drag, because the rate at which viscous work is done is determined, in a standard Kolmogorov cascade picture, by the largest scale velocities of the flow. However, polymer-enhanced viscous stresses are significant only on the small scales; which satisfy the Zimm time criterion $\omega_z < V(\ell)/\ell$. Larger eddys, for which $V(\ell)/\ell < \omega_z$, are unaffected by the presence of polymers. However it must be noted that momentum transport in bounded shear flows is critically sensitive to the dynamics of such small scale eddys immediately outside the viscous sublayer.

It is evident from the data (Figure 1-1) that polymer additives do not affect the onset of turbulence. This is probably due to the fact that the unstable sheared flows which commonly preceed the onset of turbulence rotate

polymer chains but do not stretch them. Their effect is felt in turbulent flow, which, for these data, occurs when $Re \geq 2500$. At such high Reynolds numbers turbulence is expected to be fully developed, and manifest a cascade of turbulent energy. Yet, as just discussed, the properties of such a cascade (except for the location in k-space of its inner scale) are independent of the magnitude of the viscosity. These properties include the dissipation rate, which is determined by the flow at the outer (largest) scale, and whose volume average is proportional (by conservation of energy) to the global flow drag or friction factor.

The (Kolmogorov) cascade model must therefore be modified for polymer solutions. One possible modification is simply in the numerical coefficients. The Kolmogorov analysis is entirely dimensional, and cannot determine the coefficients. It is plausible that the non-Newtonian, anisotropic, and hysteretic nature of the viscosity of a polymer solution changes the effective values of the coefficients. This possibility can be tested by detailed numerical simulation of turbulence in such fluids.

A second possibility is that the spatial variation in the effective viscosity of polymer solution pipe flow is essential. In this scenario, advanced by Lumley[7], polymers in the boundary layer are thought to be stretched and extended by inertial range eddys! As a result of the ensuing coil-stretch transition, the viscosity increases dramatically. It is important to keep in mind that this buffer-layer region of enhanced viscosity is located immediately next to the viscous sublayer, and extends to a distance from the wall $x = U_*/\omega_z$, thus encompassing the eddys that satisfy the Zimm criterion. As a result of the locally increased viscosity, transport of stream-wise momentum to the wall decreases (due to small scale eddy damping) and drag is thus reduced.

A third possibility is that the Kolmogorov cascade is truncated, or is even inapplicable because energy propagates up the cascade (to longer wavelengths) instead of down it, violating Kolmogorov's central assumption.

An important question not directly addressed by experiments to date is whether polymer extension is required for drag reduction. Most, but not

all, theories would predict that this is so. The prediction could be tested in experiments with sufficiently concentration solutions of short-chain polymers. At the onset of turbulence the strain rates will be insufficient for them to undergo the coil-stretch transition, and most theories will predict little drag reduction. At high Reynolds numbers and higher turbulent strain rates, there should be an onset (sudden or gradual) of drag reduction.

2.2 Polymers in Turbulent Flow

The behavior of dissolved polymers in flow fields has been the subject of an extensive literature. For example, Henyey and Rabin[11] have calculated equilibrium polymer conformations in stationary flow fields. The problem of dynamic polymer relaxation to an equilibrium state in specified stationary flow fields is considerably more complex (Rabin, Henyey and Pathria)[12]; Rabin[13]. The problem of polymers in turbulent flow fields is yet more difficult: the flow field is varying spatially and temporally, and the quantitative nature of these variations can be specified only statistically (and even this specification is both difficult and uncertain).

There are a number of models and an extensive literature on the subject of dissolved polymer response to flow fields. Two simple limiting models are the dumbell model (for example, as developed in a later chapter of this report) and the affine deformation model, in which the polymer is passively deformed following the strain tensor of the embedding fluid. It is frequently argued that a great degree of polymer extension (necessary in order that a low polymer concentration produce significant effects on the flow) requires that some component of the strain rate tensor exceed the Zimm relaxation rate of the polymer, proportional to $N^{-1.8}$ in a good solvent, where N is the number of monomers in the polymer chain. This argument has been challenged by RHP[12] who present a free energy argument which predicts a dependence proportional to $N^{-1.6}$ in good solvents. They assert that this latter form is in better agreement with the data. Both these arguments are essentially kinetic, in that they depend on overcoming the entropic barrier

to full polymer extension; in any significant stationary extensional flow field the equilibrium state of a long polymer is nearly fully extended. This follows from the Kramers potential describing the tendency of the viscous drag force to distend the polymer, which varies as R^3, a steeper dependence than the entropic forces which tend to keep it coiled. For small extensions (coiled polymers) R is small and the entropic forces dominate. The arguments differ in that the RHP argument demands that there be no entropic barrier, while the Zimm time argument demands only that the entropic barrier be ineffective (according to an approximate argument based on relaxation rates). One might question whether there can be anything like this sharp phase transition to an elongated state when the flow is highly turbulent; phase transitions are often smeared out in systems subjected to chaotic, time-dependent forces[6].

The problem of polymer extension in turbulent flow fields is particularly difficult and subtle. The principal axes of extension are changing with a characteristic decorrelation time τ_d. The flow has a fluctuating vorticity of characteristic magnitude ω, which rotates the polymers, and tends to interfere with their extension (it is for this reason that relatively little extension is obtained in pure shear flow, for which the magnitude of vorticity equals the largest component of the rate of strain tensor). Of course, for Kolmogorov turbulence, $\omega \sim \tau_d^{-1}$. At high strain rates a polymer molecule will have negligible entropic restoring forces, and will passively (affinely) follow the flow. In a stationary purely extensional flow field with the rate of strain $\partial v/\partial r$ its length will increase

$$\ell \approx \ell_o \exp\left(\frac{\partial v}{\partial r} t\right). \qquad (2-1)$$

In the turbulent flow field, after a single decorrelation time the extension will be

$$\ell \approx \ell_o \exp\left(\frac{\partial v}{\partial r} \tau_d\right), \qquad (2-2)$$

where the effects of vorticity are qualitatively included by defining τ_d in axes and along a path which follow the polymer molecule.

It is evident that the polymer extension depends very sensitively on

$$\frac{\partial v}{\partial r} \tau_d. \qquad (2-3)$$

As noted above, this quantity may be estimated, on dimensional grounds, to be of order unity for a turbulent flow. It is clear that its actual quantitative value (or rather, that of the analogous quantity in a more quantitative theory) is of great importance, and is a sensitive measure of the nature of the turbulent flow. However, it does appear unlikely that significant extension is possible in highly turbulent flows.

2.3 Drag Reduction

Very little of the extensive literature on polymers in turbulent flow actually attempts to explain why there should be a reduction in drag. The classic work of Lumley[7] argues that if polymer molecules are extended by turbulence in pipe flow, they lead to a flow in which two definitions of the laminar boundary thickness are possible - one based on the viscosity with unextended polymers, which should be applicable in the laminar viscous sublayer, and a larger value calculated from the viscosity in the turbulent region with extended polymers. He argues that between these two distances from the wall there should be a buffer layer into which the turbulence has difficulty penetrating, and thus through which momentum transfer is slow, thus reducing the wall drag. This buffer layer corresponds to the region of enhanced slip (i.e. good streamwise momentum confinement). This model is qualitatively reasonable, but is not quantitative enough to test.

Ryskin[14] describes a "yo-yo" model for affine polymer deformation in extensional flow. It appears to satisfactorily describe convergent flow in a cone. When applied to pipe flow, this model resembles Lumley's; its treatment of polymer dynamics in a specified flow field is quantitative, but its application to turbulence and its treatment of drag reduction are partly phenomenology, and partly semi-empirical fit to the data.

Tabor and de Gennes[15] (see also de Gennes[8] for more detail) present a very different model. They assume affine polymer deformation. In order to calculate the degree of extension, they assume that the fluid strain is a unique function of the length scale of the turbulence, in analogy to laminar

cone flow in n dimensions, where n is a non-integral number between 1 and 2. Each polymer molecule is assumed to be affected only be eddies of a single size. This description is peculiar and of dubious applicability because cone flow is strongly convergent and has a large (negative) divergence at its apex, while incompressible pipe flow and turbulence are divergence-free. Also, a given molecule is simultaneously subjected to turbulent eddies of all sizes, as pointed out by Ryskin[14]. Having made these assumptions, they define a new inner scale ℓ^{**} for the turbulent flow field, by equating the polymer elastic energy density to the Reynolds stress of the turbulence. By analogy with the early work of Lumley, but without further quantitative detail, they argue that the existence of this larger inner scale for the polymer - hydrodynamic turbulent flow leads to drag reduction by truncation of the Kolmogorov cascade.

The presence of extended polymers in a turbulent flow will increase the viscous dissipation in eddies of a given size, and thus increase the inner scale size of the flow. It is possible to construct a model analogous to that of Tabor and de Gennes in which the new inner scale is set by equating the viscous dissipation rate in flow about the polymer molecules to the rate of dissipation in the turbulence:

$$\rho \frac{U^3(\ell^{**})}{\ell^{**}} = c_p \dot{\gamma}^2 \eta R^3 \qquad (2-4)$$

where c_p is the number density of polymers, R their radius of gyration, $\dot{\gamma}$ the shear rate, η the solvent viscosity and ρ its density, and $U(r)$ is the characteristic velocity of eddies of size r. Following Tabor and de Gennes we write

$$R = \lambda R_o \qquad (2\text{-}5)$$

$$\lambda = \left(\frac{\ell^*}{\ell^{**}}\right)^n \qquad (2\text{-}6)$$

where ℓ^* is the length scale at which $\dot{\gamma}(\ell^*)$ equals the Zimm relaxation rate (the criterion for affine polymer deformation). Assuming Kolmogorov turbulence with dissipation rate ϵ and estimating $\dot{\gamma}(r) = U(r)/r$, a little algebra leads to

$$\frac{\ell^{**}}{\ell^*} = \chi^{\nu} \qquad (2-7)$$

3 A MODEL OF TURBULENT POLYMER HYDRODYNAMICS

3.1 The Dumbell Model

We focus our attention on the two end points of a long polymer chain, and replace its many internal degrees of freedom by a stretchable dumbell which spans the points–see Figure 3-1. Although clearly a gross oversimplification, this crude model has proven useful in studies of laminar polymeric flow[16], and leads to nontrivial modifications of homogeneous isotropic turbulence. The equations of motion of the two endpoints are assumed to be

$$\begin{aligned} \gamma\left(\frac{d\vec{r}_1}{dt} - \vec{v}_1\right) &= -\frac{\partial U}{\partial \vec{r}_1} + \vec{\zeta}_1 \\ \gamma\left(\frac{d\vec{r}}{dt} - \vec{v}_2\right) &= -\frac{\partial U}{\partial \vec{r}_2} + \vec{\zeta}_2, \end{aligned} \tag{3-1}$$

where $\vec{v}_1$ and $\vec{v}_2$ are the fluid velocities at the endpoints, $\gamma \approx \eta_s R_g$ is the Stoke's drag coefficient for the part of the polymer represented by the endpoint, and the spring potential is

$$U(\vec{r}_1, \vec{r}_2) = \frac{1}{2} K |\vec{r}_1 - \vec{r}_2|^2 \tag{3-2}$$

with $K = k_B T / R_g^2$. Although nonlinear spring potentials like that represented by Equation (1-13) are more realistic in the highly stretched regime, we shall for simplicity confine our attention to the more tractable linear case. In setting $\gamma \approx \eta_s R_g$, we make the usual assumption[4] that the fluid in the vicinity of the polymer chain is dragged along by the chain motion, so that the drag is of order the Stokes force on an object of size R_g. The functions $\zeta_1(t)$ and $\zeta_2(t)$ are thermal noise sources, with autocorrelation functions

$$< \zeta_i(t)\zeta_j(t') >= 2\gamma k_s T \delta_{ij} \delta(t - t'), \tag{3-3}$$

which serve to equilibrate the dumbell when there is no macroscopic fluid motion.

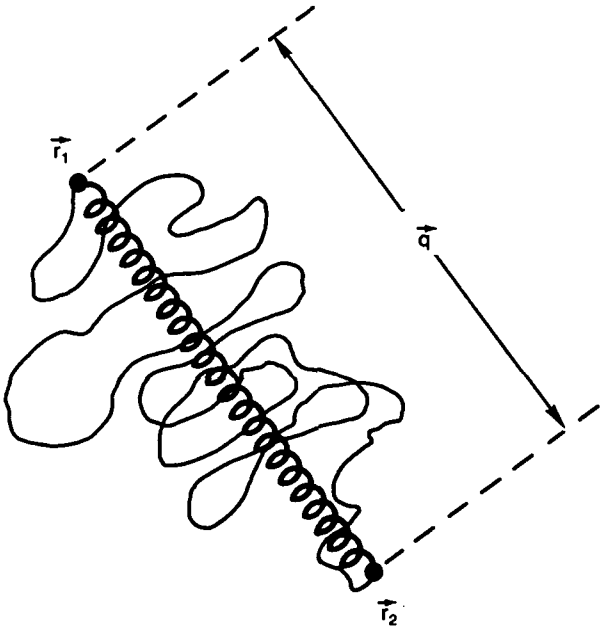

Figure 3-1. Long chain polymer with endpoints r_1 and r_2 modeled as a stretchable dumbbell.

We imagine that the fluid is filled with a dilute solution of these dumbells and pass to center-of-mass and relative coordinates for the two ends,

$$\begin{aligned} \vec{R} &= \frac{1}{2}(\vec{r}_1 + \vec{r}_2) \\ \vec{q} &= \vec{r}_1 - \vec{r}_2, \end{aligned} \tag{3-4}$$

in terms of which the Langevin Equation (3-1) may be written

$$\begin{aligned} \frac{d\vec{R}}{dt} &= \vec{v} + \frac{1}{2\gamma}[\zeta_1(t) + \zeta_2(t)] \\ \frac{d\vec{q}}{dt} &= (\vec{q}\cdot\vec{\nabla})\vec{v} - \frac{2}{\gamma}\frac{\partial U}{\partial \vec{q}} + \frac{1}{\gamma}[\zeta_1(t) - \zeta_2(t)]. \end{aligned} \tag{3-5}$$

Here $\vec{v}$ is the external velocity field evaluated at the center-of-mass position, and we have expanded $\vec{v}_1 - \vec{v}_2$ in gradients of the velocity field at this point to get Equation (3-5). Standard methods[17] then lead to a Fokker-Planck equation for the distribution function $f(\vec{R}, \vec{q}, t)$ describing the midpoints and end-to-end distances of the ensemble of dumbells, namely

$$\begin{aligned} \frac{\partial f}{\partial t} = &- \frac{\partial}{\partial \vec{R}}\cdot\left[\left(\vec{v} - D_o\frac{\partial}{\partial \vec{R}}\right)f\right] \\ &- \frac{\partial}{\partial \vec{q}}\cdot\left[\left((\vec{q}\cdot\vec{\nabla})\vec{v} - \frac{2}{\gamma}\frac{\partial U}{\partial \vec{q}} - D_q\frac{\partial}{\partial q}\right)f\right] \end{aligned} \tag{3-6}$$

where f is normalized so that

$$\int d^3R \int d^3q f(\vec{R}, \vec{q}, t) = 1. \tag{3-7}$$

The diffusion constants D_o and D_q arise from the Langevin noise sources, and are given by

$$\begin{aligned} D_o &= k_B T/2\gamma \\ D_q &= 2k_B T/\gamma. \end{aligned} \tag{3-8}$$

In a steady homogeneous shear flow parametized by the constant matrix

$$\partial_i v_j \equiv \alpha_{ij}, \tag{3-9}$$

one can check that

$$f_o(\vec{R}, \vec{q}) = \exp\left[-(u(\vec{q})/k_B T) + \alpha_{ij} q_i q_j\right] \tag{3-10}$$

is a steady state solution of (3-6).

Hydrodynamic equations follow from taking various moments of Equation (3-6). The concentration $c(\vec{r},t)$ of dumbells

$$c(\vec{r},t) = \int d^3q f(\vec{r},\vec{q},t) \qquad (3-11)$$

for example, obeys the equation

$$\partial_t c + (\vec{v}\cdot\vec{\nabla})c = D_o\nabla^2 c. \qquad (3-12)$$

An initially inhomogeneous dumbell distribution subjected to homogeneous isotropic turbulence will be mixed to uniformity in a few eddy turnover times. Henceforth, we neglect the complication of inhomogeneities in the polymer concentration, and simply set

$$c(\vec{r},t) \equiv c_P \sim \text{const.} \qquad (3-13)$$

It is also illuminating to take the first moment of Equation (3-6) and consider the dynamics of the average end-to-end distance

$$\vec{Q}(\vec{r},t) = \int d^3q\vec{q} f(\vec{r},\vec{q},t) \qquad (3-14)$$

which satisfies

$$\partial_t\vec{Q} + (\vec{v}\cdot\vec{\nabla})\vec{Q} = (\vec{Q}\cdot\vec{\nabla})\vec{v} - 2\omega_z\vec{Q} + D_q\nabla^2\vec{Q} \qquad (3-15)$$

with $\omega_z = K/\gamma$. In addition to the usual streaming and diffusive terms, there is a line stretching term $(\vec{Q}\cdot\vec{\nabla})\vec{v}$. This tendency of velocity gradients to stretch the dumbells is resisted by the term $-2\omega_z\vec{Q}$, where ω_z is of order the reciprocal of the Zimm relaxation time discussed in Section 1.0.

Equation (3-15) is in fact inappropriate for the problem at hand; to see this, note first that, as shown in Figure 3-2, many <u>different</u> polymers will interact with a given volume of fluid. Any attempt to define a hydrodynamic field $\vec{Q}(\vec{r},t)$ by averaging polymer stretching vectors over this volume will depend on purely arbitrary conventions such as whether we set $\vec{q} = \vec{r}_1 - \vec{r}_2$ or $\vec{q} = \vec{r}_2 - \vec{r}_1$ for a given dumbell. If one eliminates the ambiguity by, say, using polymers which are deuterated at one end, the configuration $\vec{q}$ will be

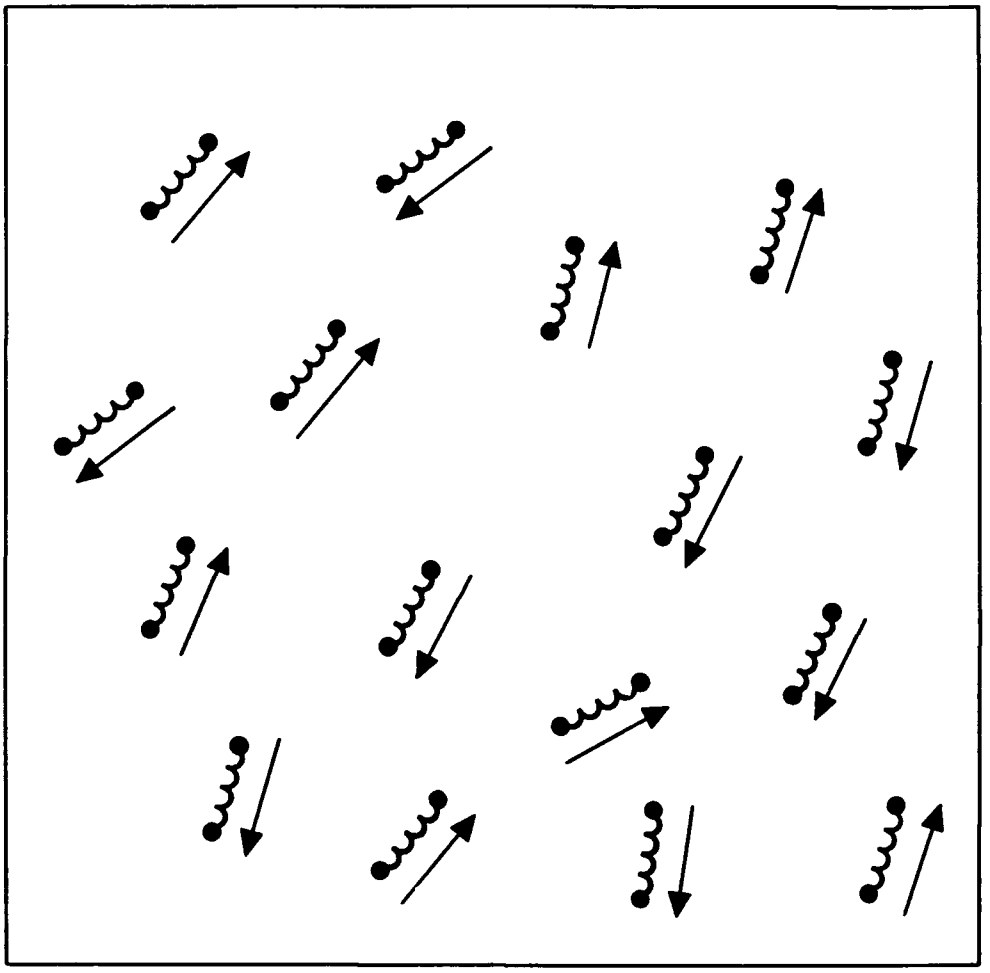

Figure 3-2. Elongated dumbbells in a hydrodynamic averaging volume, together with the microscopic stretching vectors $\{\vec{q}^{\,\alpha}\}$. The appropriate order parameter describing the state of alignment is $Q_{ij} = \langle q^{\alpha}_i q^{\alpha}_j \rangle$. The sense of the arrows depends on a arbitrary convention, which drops out with this definition of the order parameter.

as likely as $-\vec{q}$, and the hydrodynamic average $\vec{Q}(\vec{r},t)$ will be zero, even if the stretched polymers are aligned! The same problem appears in nematic liquid crystals, which are fluids of aligned rod-shaped molecules with inversion symmetry[18]. As in the case of nematics the appropriate hydrodynamic field is a tensor,

$$Q_{ij}(\vec{r},t) = \int d^3q q_i q_j f(\vec{r},\vec{q},t), \qquad (3-16)$$

which is manifestly invariant under $\vec{q} \rightarrow -\vec{q}$. The equation of motion which follows from Equation (3-6) is

$$\partial_t Q_{ij} + (\vec{v}\cdot\vec{\nabla})Q_{ij} = Q_{i\gamma}\partial_\gamma v_j + Q_{i\gamma}\partial_\gamma v_j - 4\omega_z Q_{ij} + D_o\nabla^2 Q_{ij} + \frac{4k_BT}{\gamma}\delta_{ij}. \qquad (3-17)$$

In addition to streaming, stretching and diffusive terms similar to those appearing in Equation (3-15), there is a thermal forcing contribution $(4k_BT/\gamma)\delta_{ij}$. This term balances against the Zimm relaxation term $-2\omega_z Q_{ij}$ in a uniform quiescent fluid to give the expected equilibrium solution of (3-17), namely

$$Q_{ij} = \frac{k_BT}{K}\delta_{ij} = R_g^2\delta_{ij} \qquad (3-18)$$

corresponding to an isotropic distribution of polymers with size R_g.

The tensor $Q_{ij}(\vec{r},t)$ determines how the stretched polymer distribution reacts back on the fluid. Taking over the analysis for laminar polymeric flow in Reference [16], we find that the equation of motion for the (incompressible, $\vec{\nabla}\cdot\vec{v} = 0$) velocity field is

$$\rho\left[\frac{\partial v_i}{\partial t} + (\vec{v}\cdot\vec{\nabla})v_i\right] = -\nabla_i p + c_p K\partial_j Q_{ij} + \eta\nabla^2 v_i. \qquad (3-19)$$

The new term, $c_P K\partial_j Q_{ij}$, is proportional to the concentration of polymers and represents a contribution to the fluid stress tensor of the form

$$\delta\sigma_{ij} = c_p K Q_{ij}. \qquad (3-20)$$

As explained in [16], it arises from the forces exerted on the fluid by dumbells which pierce the walls of the hydrodynamic averaging volume.

Equations (3-17) and (3-19) comprise a nontrivial hydrodynamical model of polymeric fluids which would be very interesting to study at high Reynold's

numbers via computer simulations. Except for its tensorial character (Q_{ij} has six independent components), Equation (3-17) is like the equation which describes the stretching of the magnetic field in magnetohydrodynamics (MHD)[19]. We expect that numerical codes developed for MHD could be readily adapted to study polymer hydrodynamics (PHD!). Although nonlinear dumbell springs are easily incorporated into the velocity equation, such nonlinearities lead to an infinite hierarchy of equations for moments involving $\vec{q}$, which are less straightforward to simulate. When $Q_{ij} \propto \delta_{ij}$, as in Equation (3-18), the polymeric effects can be incorporated into an additional (osmotic) contribution to the total pressure. More generally, however, we must decompose Q_{ij} into diagonal and traceless parts,

$$Q_{ij}(\vec{r},t) = Q_o(\vec{r},t)\delta_{ij} + \tilde{Q}_{ij}(\vec{r},t) \qquad (3-21)$$

where $Tr\tilde{Q}_{ij} = 0$, and observe that $\tilde{Q}_{ij}$ contributes in a nontrivial way to the dynamics of an incompressible fluid. The isotropic and traceless parts of Q_{ij} are coupled together in Equation (3-17) by the stretching terms.

Some insight into the behavior of turbulent polymeric fluids follows from the observation that, in the absence of dissipation and thermal forcing, only the sum of the fluid kinetic energy and polymer potential energy is conserved. Indeed, it is straightforward to show from Equations (3-17) and (3-19) that if

$$E_{TOT} = \frac{1}{2}\int d^3r[\rho v^2 + c_p K Q_{kk}], \qquad (3-22)$$

then

$$\frac{dE_{TOT}}{dt} = -\int d^3r[\rho\nu(\partial_i v_j)^2 + 4\omega_z Q_{kk}] \qquad (3-23)$$

where d^3r is the volume of the sample. We imagine that the macroscopic forcing of the kinetic degrees of freedom has been turned off and ask how the energy decays. Under circumstances such that the polymers are only slightly stretched, $\frac{1}{2}\ c_P K Q_{kk}$ is a negligible fraction of the kinetic energy and the conventional Kolmogorov cascade picture should be at least approximately correct. We argued, however, in Section 1.0 that eddies with characteristic size $\ell < \ell^* = (\epsilon/\omega_z^3)^{\frac{1}{2}}$ would produce effectively uniform random shears which would strongly distort the polymers. The same criterion emerges from comparing the Kolmogorov estimate of the stretching matrix $(\partial_i v_j)$ with

the Zimm rate $-\omega_z$ on the right-hand side of Equation (3-17). Because of their coiled equilibrium state, polymers are capable of enormous extensions and their potential energy can become a significant fraction of the total energy in the flow. One "viscoelastic" scenario[8],[15] is that kinetic and potential energy are exchanged between the fluid and polymer degrees of freedom over a range of scales $\ell_d < \ell < \ell^{**} < \ell^*$ in a way which effectively truncates the propagation of the kinetic energy down to the Kolmogorov inner scale. Energy is then destroyed at a slower rate by the dissipative terms on the right-hand side of Equation (3-23), because the average value of $\rho\nu(\partial_i v_j)^2$ decreases. If this effect of adding polymers is larger than the increased dissipation caused by the Zimm term $\omega_z Q_{kk}$, energy will decay at a slower rate and the drag will go down.

Tests and elaborations of these ideas via spectral closure methods and direct numerical simulations would clearly be very desirable. The scenario of Tabor and DeGennes described in Section 2.0, in particular, could be tested explicitly. The "viscoelastic" range of length scales they propose bears some similarity to a range of energy equipartition between magnetic and kinetic degrees of freedom which occurs in models of turbulent MHD, mediated by Alfven waves[20]. Equations (3-17) and (3-19) do, in fact, admit "polymer wave" solutions which are similar to Alfven waves. To see this, we first imagine that random stretching by the turbulent velocity field on scales $\ell < \ell_z$ has momentarily aligned the dumbells, as in Figure 1-3. This is like the generation of a local region of intense magnetic field in MHD. We then look for excitations out of this state of alignment which couple to the velocity field. We write the tensor Q_{ij} as

$$\begin{aligned} Q_{ij} &\approx (Q_{oi} + \delta Q_i)(Q_{oj} + \delta Q_j) \\ &\approx Q_{oi}Q_{oj} + Q_{oi}\delta Q_j + \delta Q_i Q_{oj} \end{aligned} \tag{3-24}$$

with $\vec{Q}_o \perp \delta\vec{Q}_o$, and look for normal modes of (3-17) and (3-19) of the form

$$\begin{aligned} \delta\vec{Q} &= \delta\vec{Q}_o e^{i\vec{k}\cdot\vec{r}-iwt} \\ \vec{v} &= \vec{v}_o e^{i\vec{k}\cdot\vec{r}-iwt} \end{aligned} \tag{3-25}$$

with $\delta\vec{Q}\cdot\vec{k} = \vec{v}_o\cdot\vec{k} = 0$. For wavevectors k such that $\ell_z^{-1} < k < (\ell_d)^{-1}$, we can neglect both the viscous damping and the relaxation terms in Equation

(3-17) and find the characteristic frequency

$$w(k) = \sqrt{\frac{c_p K}{\rho_o}(\vec{Q}_o \cdot \vec{k})^2}. \qquad (3-26)$$

We have assumed that the local alignment produces a Q_o which greatly exceeds R_g, so that the forcing term in Equation (3-17) can also be neglected.

For the above calculation to be meaningful, the frequency Equation (3-26) must be higher that the inverse turnover time of the eddy which produced the region of alignment, i.e., we require

$$w(k) > \epsilon^{\frac{1}{3}} k^{\frac{2}{3}}. \qquad (3-27)$$

In the region of wavevectors where this happens, kinetic energy will convert into potential energy during the lifetime of the aligned region, and the conventional Kolmogorov cascade will be modified or terminated. To calculate where this region occurs, we must evaluate Equation (3-26), and hence estimate the root mean square stretching Q_o on a scale $\ell \sim k^{-1}$ due to all relevant larger scales. Following heuristic methods developed for MHD turbulence[20], we write this as

$$Q_o^2(k) = \frac{4\pi}{3} \int_{(\ell_z)^{-1}}^{\ell^{-1}} dk k^2 \hat{Q}_{ii}(k) \qquad (3-28)$$

where

$$\hat{Q}_{ii}(k) = \int d^3 r e^{i\vec{k}\cdot\vec{r}} Q_{ii}(\vec{r}) \qquad (3-29)$$

and where the lower limit arises because scales $\ell > \ell_z$ have no effect on the polymers. Knowing the function $Q_o(k)$ is equivalent to knowing the exponent n in Equation (2-8). Simulations of Equations (3-17) and (3-19) would help test this picture, and determine the exponent n.

3.2 Polymer Hydrodynamic Turbulence

Having described the dumbell model of polymer hydrodynamics, we now turn to a discussion of the dynamics of turbulent polymer solutions. While bounded pipe and channel flows are of ultimate interest, we here focus on

the simpler (yet quite formidable) problem of understanding the physics of homogeneous polymer hydrodynamic turbulence produced by the flow of the solution thru a fine grid (hereafter referred to as grid turbulence). Our approach is to exploit the formal analogy between polymer hydrodynamics and magnetohydrodynamic turbulence, the essential physics of which is summarized in Appendix A. As noted previously, the polymer hydrodynamic extension field Q is analogous to the magnetic field $\vec{B}$, so that polymer elastic waves, which propagate at $V_E = (C_p K\ Q^2/\rho_o)^{1/2}$ are the formal counterpart of Alfven waves, which propagate at $V_A = (B_o^2/\rho_o)^{1/2}$. An important difference between the two systems occurs in the scale dependence of the dissipation. In the case of magnetohydrodynamics, magnetic energy is dissipated by resistive diffusion, so that ηk^2 characterizes the damping rate of $\vec{B}_{\underline{k}}$. In contrast, dissipation of elastic energy occurs at the Zimm relaxation rate ω_z, which is scale independent. Hence, while the magnetic Reynolds number $R_M(\ell) = \ell V(\ell)/\eta$ decreases with eddy scale size ℓ, the analogous 'elastic' Reynolds number $R_E(\ell) = V(\ell)/\ell\omega_z$ actually increases as ℓ decreases, until the rather feeble effects of polymer-concentration diffusivity assert themselves at microscopic scales (i.e. typically $D_o \ll \nu$, where ν is the fluid kinematic viscosity). Hence, dissipative effects associated with polymer dynamics are most important for scales which marginally satisfy the Zimm criterion (i.e. scales ℓ such that $V(\ell)/\ell \sim \omega_z$), and decrease in importance throughout the remainder of the inertial range.

In the production of grid turbulence, solution flows thru a hot wire grid of mesh spacing L at velocity V_o. Turbulence then evolves (rapidly) as the fluid flows downstream of the grid (i.e. see Figure 3-3). The downstream evolution of polymer hydrodynamic turbulence may be considered to occur in two sequential stages:

1. the elastization phase[21],[22],[23] — a transient phase during which the heretofore hydrodynamically 'passive' polymer coils are stretched, so that some of the mechanical energy of inertial range eddys is converted into polymer elastic energy.

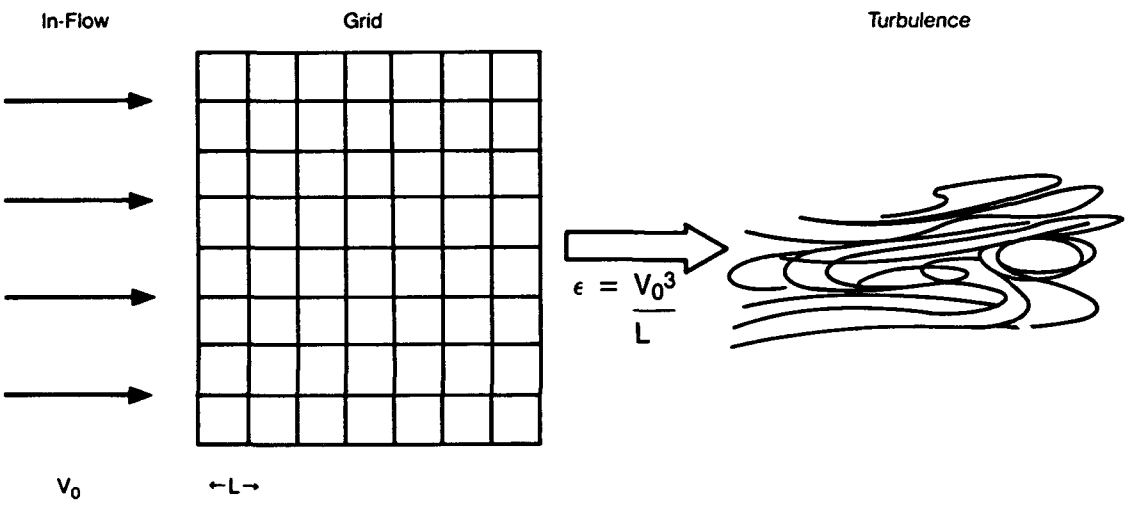

Figure 3-3. The Production and Evolution of Grid Turbulence.

2. the viscoelastic turbulence phase[20],[24] — the stage of fully developed viscoelastic turbulence during which the coupling of hydrodynamic eddys to elastic waves modifies the spectrum and energy dissipation rate of the turbulence. Throughout this discussion, it is important to keep in mind that the turbulence is <u>forced</u> at the constant rate $\epsilon = V_o^3/L$. Hence, ϵ should be thought of as a forcing rate, rather than as a "dissipation rate," its usual meaning. The actual dissipation rate will be computed using

$$\frac{dE_{TOT}}{dt} = -\int d^3r \left\{ \rho_o \nu (\underline{\nabla}\, \underline{\tilde{V}})^2 + 2\omega_z\, Q^2 \right\}. \qquad (3-30)$$

Also, it is understood that the turbulence dynamics are modified only on scales for which the Zimm criterion is satisfied (i.e. for which $V(\ell)/\ell > \omega_z$).

In the elastization phase, passive, initially coiled polymers are stretched by turbulent eddys. Since

$$\frac{d\underline{\underline{Q}}}{dt} = \underline{\underline{Q}} \cdot \underline{\nabla}\, \underline{V} - \omega_z\, \underline{\underline{Q}} \qquad (3-31)$$

it follows that the rate of polymer stretching due to eddys of scale ℓ is given by

$$\left(\frac{dQ}{dt}\right)_{\text{stretch}} \approx \frac{V(\ell)}{\ell} Q - \omega_z\, Q. \qquad (3-32)$$

Thus, perturbations in the elasticity field Q grow exponentially (on all scales for which the Zimm criterion is satisfied) at the rate $V(\ell)/\ell \sim \epsilon\, \ell^{-2/3}$. For Kolmogorov turbulence, small scale elasticity field perturbations grow most rapidly. Of course, for $\ell < \ell_d$ the growth rate drops, as such scales fall into the hydrodynamic dissipation range. This process of eddy-stretching induced growth of elasticity perturbations continues until the back-reaction of elastic energy, induced by tension in the polymer strands, becomes comparable to the mechanical energy of the stretching eddy. Thus, elastic energy growth is limited by equipartition, so that

$$c_p K\, Q_{\text{rms}}^2 \stackrel{\leq}{=} \rho_o V_o^2 (\ell_z/L)^{2/3}. \qquad (3-33)$$

Equation (3-33) assumes $\ell_z < L$, where $\epsilon^{1/3}/\ell_z^{2/3} \sim \omega_z$, i.e. the largest activated scale of Q.

In the ensuing phase of fully developed viscoelastic turbulence, two types of excitations co-exist in the polymer solution. The first are (low frequency) fluid eddys, with $\omega(\ell) \sim V(\ell)/\ell$. The second are (high frequency) elastic waves, with $\omega(\ell) \sim \tilde{V}_E/\ell$. Here $\tilde{V}_E$ is the shear elastic wave velocity computed using $Q_{\rm rms}$, i.e.

$$\tilde{V}_E^2 = C_p K \, Q_{\rm rms}^2/\rho_o. \qquad (3-34)$$

As $\tilde{V}_E$ contains contributions from all eddys with $\ell < \ell_z$, $\tilde{V}_E > V(\ell)$ for $\ell < \ell_z$. This state of viscoelastic, polymer hydrodynamic turbulence is closely analogous to magnetohydrodynamic turbulence, the basic properties of which are summarized in Appendix A. As in the case of MHD turbulence, elastic waves tend to impede inertial range transfer, since eddy interaction can occur only when two neighboring elastic waves propagating in opposite directions collide[14], generating a low frequency virtual mode which interacts with the fluid eddys (see Figure 3-4). Consequently, as in MHD, the inertial range transfer rate for viscoelastic turbulence is reduced[20], i.e.

$$1/\tau(\ell) \rightarrow \frac{V(\ell)}{\ell}\frac{V(\ell)}{\tilde{V}_E}. \qquad (3-35)$$

Hence, self-similarity of energy transfer implies $V(\ell) = (\epsilon\tilde{V}_E)^{1/4}\ell^{1/4}$ and

$$E(k) = (\epsilon\tilde{V}_E)^{1/2}k^{-3/2}, \qquad (3-36)$$

where $E_k \sim E_Q \sim E(k)$. Note that the inertial range spectrum of PHD turbulence is $\sim k^{-3/2}$ (as in MHD) rather than the familiar $k^{-5/3}$ of the Kolmogorov theory. Furthermore, the dissipation scale of PHD is also different from that of Kolmogorov turbulence and, following the arguments of Appendix A, is easily seen to be

$$\ell_{d_p} = (\tilde{V}_E/\epsilon)^{1/3}\,\nu^{2/3} \qquad (3-37)$$

Perhaps the most basic question one can ask about PHD grid turbulence is: does adding the polymers increase or decease the rate of energy

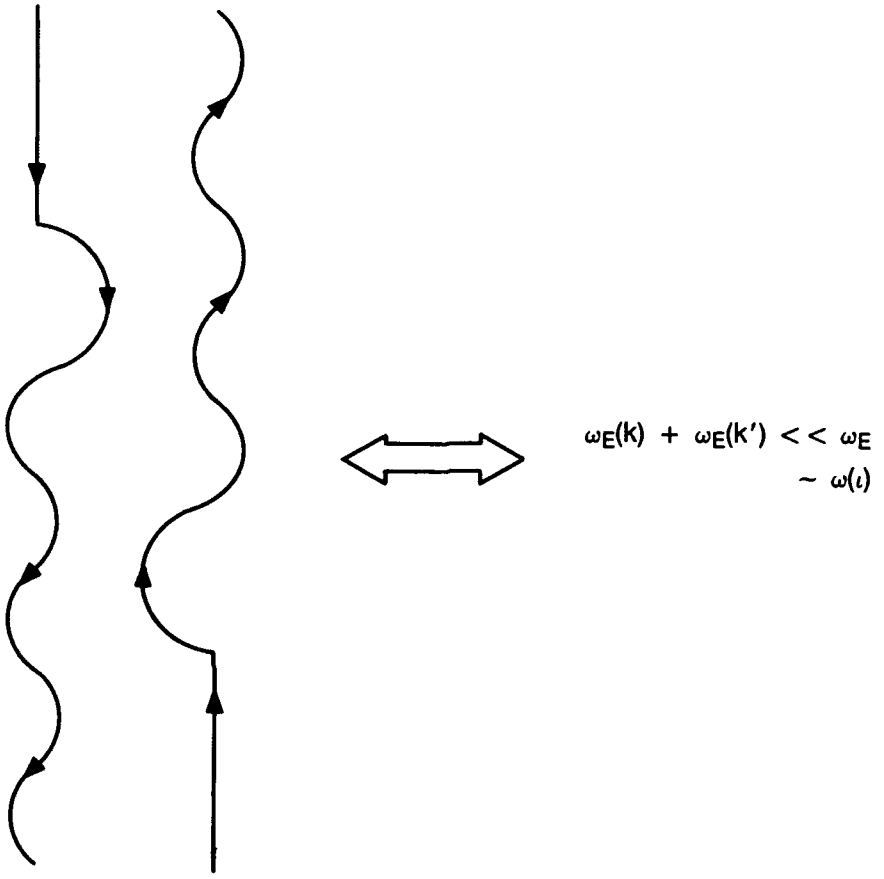

Figure 3-4. Eddy — Elastic Wave Interaction.

dissipation?! This question can now be answered by simply computing the difference of the energy dissipation rates for PHD turbulence and ordinary hydrodynamic turbulence, i.e. by calculating:

$$\begin{aligned} \Delta\epsilon &= \int_{k_z}^{k_{d_p}} \left(\nu k^2 E_k(k) + 2\omega_z E_Q(k)\right) \\ &- \int_{k_z}^{k_d} \nu k^2 E(k). \end{aligned} \tag{3-38}$$

Here, E_k and E_Q are the (equipartitioned) mechanical and elastic energies which add to the result given in Equation (3-36), $k_{d_p} = \ell_{d_p}^{-1}, k_d = (\nu^3/\epsilon)^{1/4}$ (the Kolmogorov microscale), $k_z = \ell_z^{-1}$, and $E(k) = \epsilon^{2/3}k^{-5/3}$. Note that the lower bound of the range of integration is k_z in each case, since only those scales on which the polymers are 'activated' can exhibit altered dynamics and dissipation rates. Straightforward arithmetic indicates that:

$$\Delta\epsilon > 0 \tag{3-39}$$

so that the net dissipation rate is increased! The key effect in determining that $\Delta\epsilon > 0$ is that Zimm relaxation-mode-induced dissipation is not 'small' for scales with $\ell \lessapprox \ell_z$ (i.e. see Figure 3-5), as is viscous dissipation. Alternatively put, energy must be dissipated in fluid-polymer friction drag during the process of stretching the polymer. It should also be mentioned that more detailed polymer models would consist of a spectrum of Zimm relaxation modes, each with a corresponding relaxation frequency. In that case, one might expect increased Zimm dissipation losses, since a broad spectrum of dissipation modes (rather than just one) would resonate with the fluid eddys. If a sufficient number of relaxation modes were excited the cascade could be effectively truncated. Finally, we note that the prediction that $\Delta\epsilon > 0$ should be amenable to experimental examination.

At first glance, the result of Equation (3-39) seems disturbing, since drag is predicted to increase! However, in interpreting the result one must keep in mind the important differences between grid turbulence and pipe flow turbulence. In particular, the results of the above analysis suggest that in a pipe flow a viscoelastic buffer layer will form in the region $x_V < x < x_z = U_*/\omega_z$ of the turbulent boundary layer (see Figure 3-6). Here $x_V = \nu/U_*$ is the

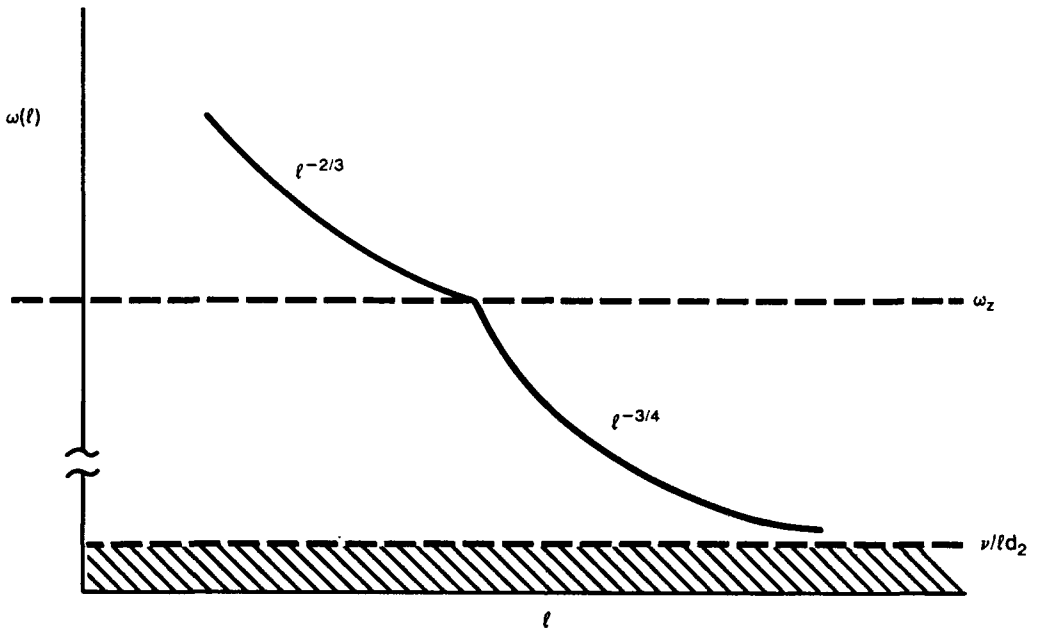

Figure 3-5. The Spectrum of Inertial Range Transfer Rates.

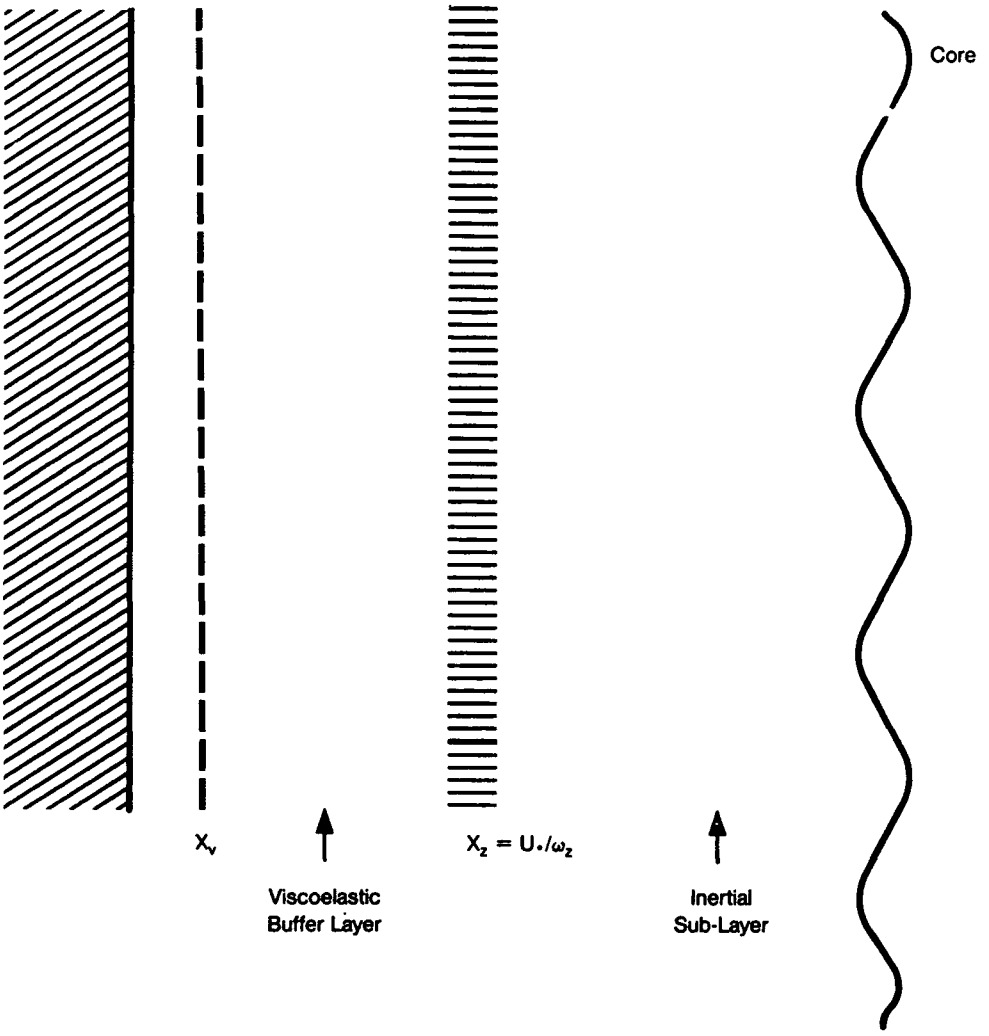

Figure 3-6. The Viscoelastic Boundary Layer.

width of the viscous sublayer. Within this viscoelastic buffer layer, all eddys satisfy the Zimm activation criterion, and thus one can expect a modified inertial range spectrum and, most importantly, enhanced dissipation in the layer. The enhanced dissipation in turn results in reduced momentum transport, and thus in enhanced slip and drag reduction. We note that this scenario is, in effect, a variation on the 'Newtonian plug and buffer layer' scenario of Lumley, with enhanced dissipation entering via ω_z rather than thru augmented viscosity. Unlike the Lumley[7] scenario, our model does not require the incidence of a coil-stretch transition. It should also be mentioned that like the model of DeGennes and Tabor[8],[15], our model predicts an equipartition of turbulent mechanical and elastic energy. It does not, however, predict a 'truncated' cascade, but rather a modified, viscoelastic cascade. Finally, it should be mentioned that our model fails to account for the observed anisotropy of inertial range eddys in drag reduced flows and for the relation of this phenomenon to the observed decorrelation of streamwise and cross-stream velocity fluctuations and thus to drag reduction. A possible resolution of this deficiency may come from the proper treatment of the small scale turbulence dynamics in the presence of a strongly sheared mean flow.[25],[26]

4 CONCLUSIONS AND RECOMMENDATIONS

4.1 Conclusions

In this report, we have surveyed the existing experimental and theoretical understanding of drag reduction by polymer additives, and have presented a new continuum model (polymer hydrodynamics — PHD) of turbulent polymer solutions. Several natural extensions of and directions for further development of this model are apparent. These include:

1. the application of standard perturbative closure methods (D.I.A., etc.)[27] to the PHD equations to develop tractable spectrum evolution equations for PHD turbulence.

2. investigation of PHD turbulence in actual bounded shear flow configurations. This would probably develop as a continuation of 1., above.

3. the generalization of the PHD model to incorporate non-Hookean elastic effects[16].

4. an investigation of the coil-stretch transition in the context of a dynamically relevant chaotic or turbulent flow.

It is clear that the study of drag reduction in turbulent polymer hydrodynamics is a difficult yet fascinating enterprise!

4.2 Program Recommendations

We believe that the time is right for an experimental and theoretical program to understand the detailed mechanics of polymer drag reduction. Such a program would consist of several parts:

1. Measurement of the velocity and strain rate correlation functions and polymer properties (extension and orientation) of turbulent polymer solution, which are homogeneous but are not driven at an outer scale; homogeneous turbulence which is driven in a Kolmogorov cascade from an outer scale; and pipe wall turbulence.

2. Measurement of drag, turbulence, and velocity structure in pipe flows selectively injected with polymers, to determine which effects of polymers are important: creation of a buffer layer, modification of the properties of the turbulence in the fully turbulent fluid, or others.

3. An extensive program of numerical simulation of turbulent polymer solutions and pipe flows, such as that already underway at the La Jolla Institute. It is also possible to make diagnostic measurements (such as of the Lagrangian strain rate and velocity autocorrelation functions) which would be very difficult in the laboratory. The great flexibility and versatility of these methods, complementing real laboratory experiments, makes them powerful and useful tools.

4. Theory to understand and interpret the results of laboratory and numerical experiments.

On account of the difficulty, complexity, and importance of polymer drag reduction phenomena this work will require the level of sophistication in experiment and theory which are the state-of-the-art in hydrodynamics, plasma physics, continuum mechanics and computational physics. It will need to draw in established professionals from those fields.

A BASIC PHENOMENOLOGY OF MHD TURBULENCE

In this Appendix, we summarize the basic phenomenology of MHD turbulence essential to our discussion of polymer-hydrodynamics. The most significant feature of MHD turbulence is the modification of the inertial range spectrum due to the presence of 'large' scale magnetic perturbations. The effect of such magnetic perturbations is to inhibit inertial range transfer by coupling small eddys to Alfven waves which propagate along the large scale magnetic perturbations. This transfer-inhibition is commonly referred to as the Alfven effect[20].

Here, we present a heuristic derivation of the Alfven effect by exploring the effect of a uniform magnetic field $\underline{B} = Bo\hat{z}$ on inertial range transfer. For the $\underline{k}$ mode, the MHD equations are:

$$\begin{aligned} \frac{\partial \tilde{\underline{V}}_{\underline{k}}}{\partial t} + \left(\tilde{\underline{V}} \cdot \underline{\nabla}\, \tilde{\underline{V}}\right)_{\underline{k}} &= \frac{\underline{B}_o}{\rho_o}\frac{\partial}{\partial z}\tilde{V}_{\underline{k}} + \left(\tilde{\underline{B}} \cdot \frac{\underline{\nabla}}{\rho_o}\tilde{\underline{B}}\right)_{\underline{k}} \\ &- \frac{\underline{\nabla}}{\rho_o}\left(p + \underline{B}_o \cdot \tilde{\underline{B}}_{\underline{k}} + \tilde{\underline{B}}_{\underline{k}}^2/2\right) \end{aligned} \qquad \text{(A-1)}$$

and

$$\frac{\partial \tilde{\underline{B}}_{\underline{k}}}{\partial t} + \left(\tilde{\underline{V}} \cdot \underline{\nabla}\, \tilde{\underline{B}}\right)_{\underline{k}} = B_o \frac{\partial}{\partial z}\, \tilde{\underline{V}}_{\underline{k}} + \left(\tilde{\underline{B}} \cdot \underline{\nabla}\, \tilde{\underline{V}}\right)_{\underline{k}} \qquad (A-2)$$

Here, the inertial range transfer rate for the eddy of scale $|\underline{k}|^{-1}$ is just $1/\tau_{\underline{k}} = \left(\tilde{\underline{V}} \cdot \underline{\nabla}\, \tilde{\underline{V}}\right)_{\underline{k}}$, which we estimate using standard iterative closure methods, i.e.:

$$1/\tau_{\underline{k}} = \underline{k} \cdot \sum_{\underline{k}'} \tilde{\underline{V}}_{\underline{k}'}\, \hat{\underline{V}}^{(2)}_{\underline{k}+\underline{k}'} \qquad (A-3)$$

where:

$$\begin{aligned} \Delta\omega_{\underline{k}''}\tilde{\underline{V}}^{(2)}_{\underline{k}+\underline{k}'} - \frac{ik_z B_o}{\rho_o}\, \tilde{\underline{V}}^{(2)}_{\underline{k}''} &= \tilde{\underline{V}}_{\underline{k}'} \cdot \underline{k}\, \tilde{\underline{V}}_{\underline{k}} \\ \Delta\omega_{\underline{k}''}\tilde{\underline{B}}^{(2)}_{\underline{k}+\underline{k}'} &= B_o ik_z\, \tilde{\underline{V}}^{(2)}_{\underline{k}''}. \end{aligned} \qquad \text{(A-4)}$$

Here, the only virtual velocity-velocity interactions are retained, since we only seek to determine the effect of B_o on fluid eddy-shearing. Furthermore, for simplicity, a single parallel wave vector is assumed. Here, $\Delta\omega_{\underline{k}''}$ is the

inverse decorrelation time for the $\underline{k}+\underline{k}'$ virtual mode. Combining Equations (A-2) and (A-3) yields:

$$1/\tau_{\underline{k}} = \sum_{\underline{k}'} \frac{\left(\underline{k}\cdot\tilde{V}_{\underline{k}'}\right)^2}{\Delta\omega_{\underline{k}''}} 1/\left[1+\left(\frac{k_z V_A}{\Delta\omega_{\underline{k}''}}\right)^2\right]. \qquad (A-5)$$

Here $V_A = B_o/\sqrt{\rho_o}$ is the Alfven velocity. Enforcing locality of transfer (i.e. $\underline{k}\sim\underline{k}'$) then yields:

$$1/\tau_{\underline{k}} \sim k\tilde{V}_{\underline{k}}/\left(1+\left(\frac{k_z V_A}{\Delta\omega_{\underline{k}}}\right)^2\right)^{1/2}. \qquad (A-6)$$

In the limit $V_A \to 0$ (i.e. no magnetization), Equation (A-6) reduces to the familiar relation for Kolmogorov turbulence, i.e. $1/\tau_{\underline{k}} \sim k\tilde{V}_{\underline{k}}$. In the strong magnetization limit, $k_z V_A > \Delta\omega_k^{-1}$, Equation (A-6) implies that

$$1/\tau_{\underline{k}} \sim k\tilde{V}_{\underline{k}}\frac{\Delta\omega_{\underline{k}}}{k_z V_A}. \qquad (A-7)$$

It is apparent that a strong magnetic field (i.e. $k_z V_A \gg \Delta\omega$) acts to reduce inertial range transfer. Interpreting Equation (A-7) iteratively then yields:

$$1/\tau_{\underline{k}} \sim k\tilde{V}_{\underline{k}}\frac{\tau_A}{\tau_k^{(0)}} \sim \frac{\left(k\tilde{V}_{\underline{k}}\right)^2}{k_z V_A}. \qquad (A-8)$$

Equation (A-8) states that a strong magnetic field inhibits inertial range transfer by increasing eddy lifetimes by a factor of $k_z V_A/k\tilde{V}_{\underline{k}}$.

The result of Equation (A-8) is appropriate to the case of a DC magnetic field. Since large scale magnetic fluctuations will behave similarly, and since Alfvenic interaction is non-local in $\underline{k}$-space (note that the $\underline{J}\times\underline{B}$ force cannot be eliminated by a Galilean transformation!), we can generalize Equation (A-8) by arguing the correspondence $k_z V_A \to k\tilde{V}_A$, where $\tilde{V}_A = (\tilde{B})_{\rm rms}/\sqrt{\rho_o}$, the Alfven velocity calculated using the root-mean-square fluctuating field $\tilde{B}_{\rm rms}$, which is dominated by contributions from the large scale magnetic perturbations. In that case:

$$1/\tau_k = (k\tilde{V}_k)^2/k\tilde{V}_A, \qquad (A-9)$$

which is the well-known but heretofore unjustified result for the Alfvenically modified eddy turn-over rate appropriate to MHD turbulence.

The notion that magnetic fields inhibit inertial range interaction is frequently expressed by the alternative statement that two eddys will not interact unless they propagate in opposite directions along neighboring magnetic field lines (i.e. see Figure 3-5)[16]. This conception of the Alfven effect can be manifested in the simple model presented by relaxing the simplifying assumption of a single k_z. In that case, $k_z \rightarrow k_z + k_z'$ in Equation (A-6), which in turn implies that energy transfer will be inhibited unless $(k_z + k_z')V_A \gg \Delta\omega_{k''}$. Of course, $(k_z + k_z')V_A \rightarrow 0$ is mathematically equivalent to the physical picture that two Alfven waves propagate in opposite directions. It is also interesting to note that the 'inhibition factor' $\left(1 + (k_z''\, k_A)^2/\Delta\omega^2_{\underline{k}''}\right)^{1/2}$ suggests an analogy between inertial range interaction and nonlinear Landau damping in a plasma[28], with fluid eddys as the analogue of particles and $\Delta\omega_{\underline{k}''}$ as the counterpart to the spectrum-averaged ballistic frequency $(\Delta k)V_{th}$, where V_{th} is the particle thermal velocity. From that view-point, the inhibition factor implies that wave-eddy interaction occurs when $k_z''\, V_A < \Delta\omega_{\underline{k}''}$, just as nonlinear Landau damping occurs when two waves beat to drive a 'virtual' mode which resonates with the particles, i.e. when $\omega + \omega' = \omega'' < \Delta k V_{th}$. Alternatively, just as spectral transfer due to nonlinear Landau damping is small in the ratio $(\Delta k)V_{th}/\omega$, inertial range transfer in MHD turbulence must be small in the ratio $\Delta\omega_k/k_z V_A$. In the corresponding case without a DC field, $\Delta\omega_{\underline{k}}/k_z V_A \rightarrow \tilde{V}(\ell)/\tilde{V}_A$, thus recovering Equation (A-8).

Having derived the effective eddy turn-over rate for MHD turbulence, it is straightforward to determine the modified inertial range spectrum. Balancing the dissipation rate ϵ (which is also the inertial range energy flow-thru rate) with $V(\ell)^2/\tau(\ell)$ (where $V(\ell)$ and $\tau(\ell)$ are the velocity and effective turn-over rate for an eddy of scale ℓ) yields:

$$\epsilon = \frac{V(\ell)^2}{\tau(\ell)} = V(\ell)^2 \frac{V(\ell)}{\ell} \frac{\tau_A(\ell)}{\tau(\ell)} = \frac{V(\ell)^4}{\ell \tilde{V}_A}. \qquad \text{(A-10)}$$

Thus $V(\ell) = (\epsilon \tilde{V}_A)^{1/4} \ell^{1/4}$ and hence

$$E(k) = (\epsilon \tilde{V}_A)^{1/2} k^{-3/2}. \qquad (A-11)$$

Thus, the Alfven effect changes the inertial range spectrum from $E(k) = \epsilon^{2/3} k^{-5/3}$ to $E(k) = (\epsilon \tilde{V}_A)^{1/2} k^{-3/2}$. Note that since $\tau_A(\ell) < \tau(\ell)$, inertial range mechanical and magnetic energies are equal. Similarly, the modified dissipation scale ℓ_d can be determined by balancing the modified eddy turnover rate $\tau(\ell)^{-1}$ with the viscous dissipation rate ν/ℓ^2, where ν is the kinematic viscosity. This implies:

$$\frac{\nu}{\ell_d^2} = \frac{V(\ell_d)^2}{\ell_d \tilde{V}_A} \qquad (A-12)$$

so that using the relation $V(\ell_d) = (\epsilon \tilde{V}_A)^{1/4} \ell_d^{1/4}$ yields

$$\ell_d = \nu^{2/3} (\tilde{V}_A/\epsilon)^{1/3}, \qquad (A-13)$$

which is the dissipation scale for MHD turbulence. Note that the assumption of $\nu \sim \eta$ (where η is the resistivity) is implicit in this analysis.

REFERENCES

1. B. A. Toms, Proc. 1st Int. Congress of Reology, Vol. II, p. 135 (North-Holland, 1948)

2. P. S. Virk, E. W. Merrill, H. S. Mickley, K. A. Smith, and E. L. Mollo-Christensen, J. Fluid Mech. 30, 305 (1967)

3. P. S. Virk, Al. Ch. E. Journal, 21 624 (1975).

4. H. Tennekes and J. Lumley, A First Course in Turbulence, (MIT Press, Cambridge, 1972).

5. W. D. McComb and L. H. Rabie, Phys. Fluids 22, 183 (1979)

6. P. G. de Gennes, Scaling Concepts in Polymer Physics, (Cornell University Press, Ithaca, 1984).

7. J. Lumley, J. Polymer Sci. 7, 263 (1973)

8. P. G. de Gennes, Physica 140A, 9 (1986)

9. Y. Kantor, M. Kardar, and D. R. Nelson, Phys. Rev. A35, 3056 (1987)

10. J. Isaacson and T. C. Lubensky, J. de Physique Lett. 41, L469 (1980); T. C. Lubensky and A. J. McKane, J. de Physique Lett. 42, L331 (1981)

11. F. S. Henyey and Y. Rabin, J. Chem. Phys. 82, 4362 (1985)

12. Y. Rabin, F. S. Henyey, and R. K. Pathria, Phys. Rev. Lett. 55, 201 (1985)

13. Polymer-Flow Interaction, A.I.P. Conf. Proc. 137, edited by Y. Rabin (AIP, New York, 1985).

14. G. Ryskin, J. Fluid Mech. 178, 423 (1987); Phys. Rev. Lett. 59, 2059 (1987).

15. M. Tabor and P. G. DeGennes, Europhys. Lett. 2, 519 (1986).

16. R. B. Bird, et. al., Dynamics of Polymeric Liquids Vol. II (J. Wiley and Sons, New York, 1987).

17. N. Wax, ed. Selected Papers on Noise and Stochastic Processor (Dover, New York, 1969).

18. P. G. DeGennes, The Physics of Liquid Crystals, (Oxford, New York).

19. H. K. Moffatt, Magnetic Field Generation in Electrically Conducting Fluids (Cambridge, New York, 1978).

20. R. H. Kraichnean, Phys. Fluids 8, 1385 (1965).

21. P. S. Iroshnikov, Sov. Astron. 7, 548 (1964).

22. G. K. Batchelor, Proc. Roy. Soc. A 201 349 (1950).

23. P. G. Saffman, J. Fluid Mech. 16 545 (1963).

24. R. H. Kraichnan and S. Nagarajan, Phys. Fluids 10, 859 (1967).

25. D. Biskamp, Phys. Fl. B1, 1964 (1989).

26. T. Chiueh, P.. Terry, P. H. Diamond, J. E. Sedlak, Phys. Fl. 29, 231 (1986).

27. H. Biglari, P.H. Diamond, P. W. Terry, Phys. Fluids B2, 1 (1990)

28. R. H. Kraichnan, J. Fluid Mech. 5 497 (1959).

29. R. Z. Sagdeev and A. A. Galeev, Nonlinear Plasma Theory, (Addison-Wesley, Menlo-Park, 1969).

DISTRIBUTION LIST

CMDR & Program Executive Officer
US Army/CSSD-ZA
Strategic Defense Command
PO Box 15280
Arlington, VA 22215-0150

Mr John Bachkosky
Deputy DDR&E
The Pentagon, Room 3E114
Washington, DC 20301

Dr Joseph Ball
Central Intelligence Agency
Washington, DC 20505

Dr Arthur E Bisson
DAWSD (OASN/RD&A)
The Pentagon, Room 5C675
Washington, DC 20350-1000

Dr Albert Brandenstein
Chief Scientist
Office of Nat'l Drug Control Policy
Executive Office of the President
Washington, DC 20500

Mr Edward Brown
Assistant Director
DARPA/NMRO
3701 North Fairfax Drive
Arlington, VA 22203-1714

Dr H Lee Buchanan, I I I
Director
DARPA/DSO
3701 North Fairfax Drive
Arlington, VA 22203-1714

Dr Curtis G Callan, Jr
Physics Department
PO Box 708
Princeton University
Princeton, NJ 08544

Dr Ferdinand N Cirillo Jr
Central Intelligence Agency
Washington, DC 20505

Brig Gen Stephen P Condon
Deptuty Assistant Secretary
Management Policy &
Program Integration
The Pentagon, Room 4E969
Washington, DC 20330-1000

Ambassador Henry F Cooper
Director/SDIO-D
The Pentagon, Room 1E1081
Washington, DC 20301-7100

D A R P A Library
3701 North Fairfax Drive
Arlington, VA 22209-2308

D T I C [2]
Cameron Station
Alexandria, VA 22314

Mr John Darrah
Senior Scientist and Technical Advisor
HQAFSPACOM/CN
Peterson AFB, CO 80914-5001

Dr Gary L Denman
Director
DARPA/DIRO
3701 North Fairfax Drive
Arlington, VA 22203-1714

DISTRIBUTION LIST

Dr Patrick H Diamond
6365 Cascade Street
San Diego, CA 92122

Dr Nancy Dowdy
USACDA
320 21st Street NW
Washington, DC 20451

Mr John N Entzminger
Chief Advance Technology
DARPA/DIRO
3701 North Fairfax Drive
Arlington, VA 22203-1714

Capt Kirk Evans
Director Undersea Warfare
Space & Naval Warfare Sys Cmd
Code PD-80
Department of the Navy
Washington, DC 20363-5100

Dr S William Gouse
Sr Vice President and General Manager
The MITRE Corporation
Mail Stop Z605
7525 Colshire Drive
McLean, VA 22102

Mr Thomas H Handel
Office of Naval Intelligence
The Pentagon, Room 5D660
Washington, DC 20350-2000

Maj G Hard
Director of Space and SDI Programs
Code SAF/AQS
The Pentagon
Washington, DC 20330-1000

Dr Jeffrey Alan Harvey
714 S Garfield
Hinsdale, IL 60521

Dr Robert G Henderson
Director
JASON Program Office
The MITRE Corporation
7525 Colshire Drive
Mailstop Z561
McLean, VA 22102

Dr Barry Horowitz
President and Chief Executive Officer
The MITRE Corporation
202 Burlington Road
Bedford, MA 01730-1420

Dr William E Howard I I I [2]
Director
Space and Strategic Technology Office
Assistant Secretary of the Army
The Pentagon, Room 3E474
Washington, DC 20310-0103

Dr Gerald J Iafrate
US Army Research Office
PO Box 12211
4330 South Miami Boulevard
Research Triangle Pk, NC 27709-2211

J A S O N Library [5]
The MITRE Corporation
Mail Stop W002
7525 Colshire Drive
McLean, VA 22102

Dr George Jordy [25]
Director for Program Analysis
US Department of Energy
ER30 OER
Washington, DC 20585

DISTRIBUTION LIST

Dr O' Dean P Judd
Los Alamos National Lab
Mail Stop A-110
Los Alamos, NM 87545

Dr Bobby R Junker
Office of Naval Research
Code 412
800 North Quincy Street
Arlington, VA 22217

Dr Jonathan I Katz
Department of Physics
Washington University
St Louis, MO 63130

Mr Robert Madden [2]
Department of Defense
National Security Agency
Attn: R-9 (Mr. Madden)
Ft George G Meade, MD 20755-6000

Dr Arthur F Manfredi Jr [10]
OSWR
Central Intelligence Agency
Washington, DC 20505

Mr Joe Martin
Director
OUSD(A)/TWP/NW&M
The Pentagon, Room 3D1048
Washington, DC 20301

Mr James J Mattice
Deputy Assistant Secretary
SAF/AQ
The Pentagon, Room 4D-977
Washington, DC 20330-1000

Mr. Ronald D Murphy
Director
DARPA/ASTO
3701 North Fairfax Drive
Arlington, VA 22203

Dr Julian C Nall
Institute for Defense Analyses
1801 North Beauregard Street
Alexandria, VA 22311

Dr David R Nelson
15 Hancock Street
Lexington, MA 02173

Dr Gordon C Oehler
Central Intelligence Agency
Washington, DC 20505

Dr Peter G Pappas
Chief Scientist
US Army Strategic Defense Command
PO Box 15280
Arlington, VA 22215-0280

Dr Ari Patrinos
Director
Environmental Sciences Division
ER74/GTN
US Department of Energy
Washington, DC 20585

Dr Bruce Pierce
USD(A)D S
The Pentagon, Room 3D136
Washington, DC 20301-3090

DISTRIBUTION LIST

Mr John Rausch [2]
Division Head 06 Department
NAVOPINTCEN
4301 Suitland Road
Washington, DC 20390

Records Resource
The MITRE Corporation
Mail Stop W115
7525 Colshire Drive
McLean, VA 22102

Dr Fred E Saalfeld
Director
Office of Naval Research
800 North Quincy Street
Arlington, VA 22217-5000

Dr John Schuster
Technical Director of Submarine
and SSBN Security Program
Department of the Navy OP-02T
The Pentagon, Room 4D534
Washington, DC 20450-2000

Dr Barbara Seiders [2]
Chief of Research
Office of Chief Science Advisor
Arms Control & Disarmament Agency
320 21st Street NW
Washington, DC 20451

Dr Philip A Selwyn [2]
Director
Office of Naval Technology
Room 907
800 North Quincy Street
Arlington, VA 22217-5000

Dr Paul J Steinhardt
David Rittenhouse Laboratory
Department of Physics
University of Pennsylvania
33rd & Walnut Streets
Philadelphia, PA 19104-6396

Superintendent
Code 1424
Attn: Documents Librarian
Naval Postgraduate School
Monterey, CA 93943

Dr George W Ullrich [3]
Deputy Director
Defense Nuclear Agency
6801 Telegraph Road
Alexandria, VA 22310

Ms Michelle Van Cleave
Asst Dr/National Security Affairs Office
Science and Technology Policy
New Executive Office Building
17th and Pennsylvania Avenue
Washington, DC 20506

Mr Richard Vitali
Director of Corporate Laboratory
US Army Laboratory Command
2800 Powder Mill Road
Adelphi, MD 20783-1145

Dr Edward C Whitman
Deputy Asst Secretary of the Navy
C3I Electronic Warfare & Space
Department of the Navy
The Pentagon, Room 4D745
Washington, DC 20350-5000

DISTRIBUTION LIST

Mr Donald J Yockey
U/Secretary of Defense For Acquisition
The Pentagon, Room 3E9333
Washington, DC 20301-3000

Dr Linda Zall
Central Intelligence Agency
Washington, DC 20505

Mr Charles A Zraket
Trustee
The MITRE Corporation
Mail Stop A130
202 Burlington Road
Bedford, MA 01730